Marine Micropaleontology 186 (2024) 102310

Contents lists available at ScienceDirect

Marine Micropaleontology

journal homepage: www.elsevier.com/locate/marmicro

Research paper

Origin and evolution of the Neogene calcareous nannofossil *Ceratolithus*

Carlos Lancis [a], José-Enrique Tent-Manclús [a,b,*], José-Abel Flores [c]

[a] University of Alicante, Department of Earth and Environmental Sciences, Apto. 99. 03080 San Vicente del Raspeig, Alicante, Spain
[b] University of Alicante, Multidisciplinary Institute for Environmental Studies "Ramón Margalef", Apto. 99. 03080 San Vicente del Raspeig, Alicante, Spain
[c] University of Salamanca, Department of Geology, Plaza de la Merced s/n, 37008 Salamanca, Spain

ARTICLE INFO

Keywords:
Calcareous nannofossils evolution
Ceratoliths
Ceratolithus
Late Neogene
ODP Hole 999A
ODP Site 1237
Orthorhabdus

ABSTRACT

Sediment samples of deep marine oceanic ODP boreholes from sites 999 in the Caribbean Sea and 1237 in the Eastern Pacific Ocean covering the period between 6 and 4.5 Ma have been studied with a focus on ceratolith evolution. *Orthorhabdus rugosus* is a nannolith with three blades (sinistral, median, and dextral) that first appeared during the Serravallian, it is not-birefringent in its stable orientation. It shows a high morphological variability time-interval at the end of the Messinian to the basal Pliocene (5.5 to 5 Ma) during which *Ceratolithus* (5.484 Ma) evolved. Changes occurred in the sinistral and median blades, whilst the dextral blade was reduced. *Ceratolithus finifer* n. comb is the first species of the evolutionary line. The nannolith stable position changed during its evolution, resulting in the older forms showing low birefringence and the younger ones moderate to high birefringence in the most stable orientation. *Ceratolithus acutus*, with an arrowhead shape, *Ceratolithus armatus,* and the morphologically distinct *C. larrymayeri* evolved from *C. finifer* with all three species showing high birefringence. The previous *O. rugosus* and *C. finifer* continued. Finally, *C. armatus* gives rise to *C. cristatus*. *Ceratolithus atlanticus* and *C. tricorniculatus* also evolved from *C. finifer*. All the species mentioned become extinct during the Pliocene except *Ceratolithus cristatus* that lives today. Detailed observations permit the analysis of the evolutionary trends of the group, possible mechanisms, patterns, and processes of speciation, and establish new criteria to define the species that, by their relative abundance and short geologic range, have permitted adjustment of biostratigraphic markers for this period.

1. Introduction

A distinct group of microfossils known as horseshoe-shaped nannoliths have been proven to be valuable in calcareous nannofossil biostratigraphy. The first genus of nannoliths with a horseshoe form was described by Kamptner in 1950 and was named *Ceratolithus*.

Norris (1965) study revealed that a single ceratolith is typically wrapped around the cell, and that beyond the ceratolith, a large coccosphere of hoop-shaped coccoliths can occasionally be observed. Alcober and Jordan (1997), Young et al. (1999), Cros et al. (2000), and Sprengel and Young (2000) observed *C. cristatus* and hoop-shaped coccoliths inside coccospheres of *Neosphaera coccolithomorpha* planoliths, suggesting that ceratoliths, planoliths, and hoop coccoliths may form during alternate phases of a complex life cycle (Young et al., 2005). Ceratoliths are part of the division Haptophyta (Jordan and Chamberlain, 1997), which includes the coccolithophores.

The evolutionary history and relationships within the group of ceratoliths (Ceratolithaceae) have been a subject of study and debate among researchers. In 1967, Gartner proposed that *Amaurolithus* evolved from *O. rugosus*. However, later Gartner and Bukry (1975) questioned this initial relationship. They pointed out that the earliest Ceratolithaceae species appeared in the fossil record without clear likely ancestral forms. The absence of direct ancestral forms led them to propose a different explanation for the sudden appearance of the genus in the fossil record. Gartner and Bukry (1975) suggested that ancestral forms of Ceratolithaceae might have evolved in a non-calcifying state. As a consequence, ceratoliths could appear abruptly in the fossil record without an obvious precursor with calcified structures. To further investigate the interrelationships within the group, Gartner and Bukry (1975) discussed possible lineages and constructed a phylogenetic chart (Fig. 3 in their study). They considered *A. primus* or *A. delicatus* as potential ancestral forms. They proposed a monophyletic origin, including the genus *Ceratolithus* whose first species, *C. acutus*, they suggested was derived from *A. amplificus*. Later, Perch-Nielsen (1985), Raffi et al.

* Corresponding author at: Earth and Environmental Sciences Department Alicante University Carretera San Vicente del Raspeig s/n 03690 San Vicente del Raspeig, Alicante Spain.
E-mail address: je.tent@ua.es (J.-E. Tent-Manclús).

https://doi.org/10.1016/j.marmicro.2023.102310
Received 27 February 2023; Received in revised form 30 October 2023; Accepted 13 November 2023
Available online 18 November 2023

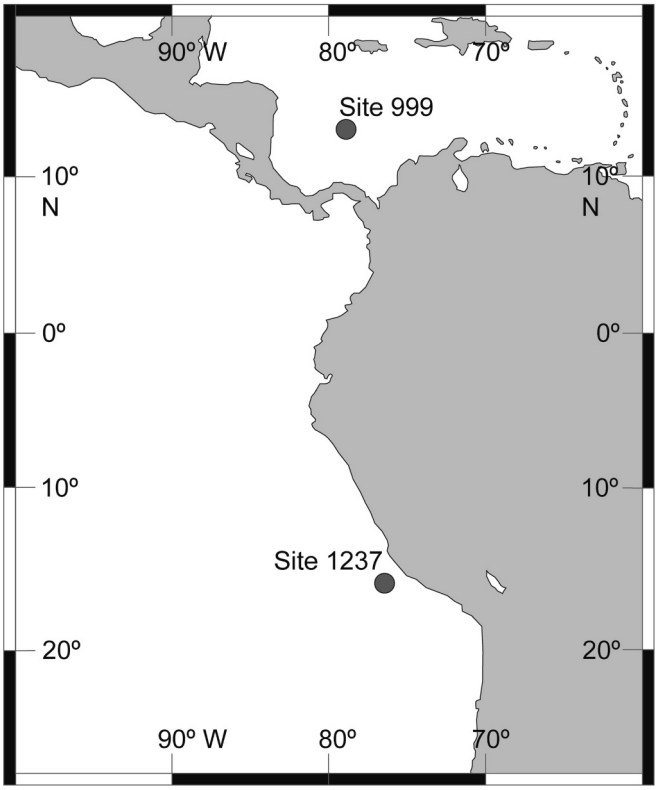

Fig. 1. Location map of ODP sites: 999 drilled during Leg 165 (12°44.639′N, 78°44.360′W, and water depth of 2827.9 m; Sigurdsson et al., 1997) and 1237 drilled during Leg 202 (16°0.421′S, 76°22.685′W, and water depth of 3212 m; Mix et al., 2003).

Table 1
Nannofossil events in ODP Hole 999A; LO: Lowest occurrence; HO: highest occurrence.

EVENT	CORE-SECTION-CM	Metres Composite Deep	AGE Ma
HO. *C. atlanticus*	17H-5W-80:**17H-**	156.90–**158.22**	5.075–**5.173**
HO *C. finifer*	**6W-90**		
LO *C. cristatus*	**18H-1W-5**:18H-1W-15	**159.65**–159.74	**5.257**–5.260
LO *C. armatus*	**18H-1W-90**: 18H-1W-145	**160.50**–160.91	**5.283**–5.299
HO *O. rugosus*	18H-1W-90:**18H-1W-145**	160.50–**160.91**	5.283–**5.299**
LO *C. tricorniculatus*	**18H-1W-145**:18H-2W-5	**160.91**–161.00	**5.299**–5.301
LO *C. larrymayeri*			
LO *C. atlanticus*	**18H-2W-90**:18H-2W-145	**161.76**–162.26	**5.322**–5.335
LO. *C. acutus*			
LO *R. cisnerosi**	**18H-5W-60**:18H-5W-5	**165.56**–165.07	**5.452**–5.430
LO *C. finifer*	**18H-5W-110**:18H-6W-60	**165.99**–166.91	**5.472**–5.523

Ages are obtained after the site calibrated depth versus age obtained by Bickert et al. (2004) and Haug and Tiedemann (1998)/ Haug et al. (2001). The event samples are indicated in bold font and the lower/upper samples in the LO/HO. The samples metres composite depth (mcd) and the early/late calibrated ages are also shown. *A circular *Reticulofenestra* species described by Lancis Sáez (1998) that marks the Early Pliocene in the Mediterranean Basin (Lancis and Flores, 2006).

(1998), Blair et al. (2017), and Lancis et al. (2022) revised the relationship within the ceratoliths group. Raffi et al. (1998) investigated the origin of *Ceratolithus* by light microscopy. They found *Triquetrorhabdulus finifer* (Theodoridis, 1984) specimens seem to have evolved into a ceratolith that is closely related to *C. acutus*. The first *Ceratolithus* occurred at approximately 5.36 Ma (Raffi et al., 2020).

Young and Bown (2014) transferred several species previously placed in *Triquetrorhabdulus* into *Orthorhabdus,* for instance *O. rugosus,* on the basis of crystallographic orientation (c-axis parallel to nannolith length in *Triquetrorhabdulus* but perpendicular to nannolith length in *Orthorhabdus*). They also transferred both genera into the Family Ceratolithaceae.

Blair et al. (2017) assumed the monophyletic origin suggested by Gartner and Bukry (1975) and proposed two new ceratolith species, *C. apiculus* and *C. cornulum*, and used *C. separatus* as defined by Bukry (1979).

The previous work of Lancis et al. (2022) about ceratolith evolution focused on the appearance of the genera *Amaurolithus* and *Nicklithus* from the *Orthorhabdus rugosus* ancestor. During the Late Messinian, *Nicklithus amplificus* and *Amaurolithus primus* became extinct, and *Amaurolithus delicatus* survived during the Early Pliocene. At the end of the Messinian and in the basal Pliocene, a second *O. rugosus* variability time-interval produced the new genus *Ceratolithus* (Raffi et al., 1998), which is the subject matter of this paper.

The genus *Ceratolithus* was investigated in this study, focusing on the phylogenetic links between the genera *Orthorhabdus* and *Ceratolithus,* with specific documentation of its origin and temporal distribution. The study was based on detailed documentation by SEM of their fossil record in continuous sedimentary sections of ODP sites 999 and 1237, which have abundant, well-preserved, and diverse nannofossils.

2. Material and methods

2.1. Site settings

Samples from two ODP sites, 999 of Leg 165, and 1237 of Leg 202, were studied. Fig. 1 shows the borehole locations. Detailed site locations for site 999, core recovery, and lithological descriptions can be found in Sigurdsson et al. (1997), and for site 1237 in Mix et al. (2003), also see description in the previous work of Lancis et al. (2022).

2.2. Sample preparation

Thirty-five smear slides comprising 182 and 151 m corrected depth (mcd) of Hole 999A and 46 samples comprising 115 mcd and 70 mcd of the composite Site 1237 were prepared in the Salamanca University Department of Geology using the decantation technique of Flores and Sierro (1997). The common spacing between samples was of 1 m but decreased in selected intervals to 0.1 m (Annex 1). The slides were examined using a polarised microscope (PM) at x1000. The focus of this work is the interval from highest occurrence (HO) of *N. amplificus* until the middle of the Pliocene after the lowest occurrence (LO) *C. cristatus*.

In addition, 25 samples from Hole 999A and 53 from composite Site 1237 were prepared at Alicante University, Department of Earth Science and Environmental Science, using a technique of centrifugation/filtration of the mentioned interval for observation with SEM (Annex 1). Using hydrogen peroxide and an ultrasound bath, samples were disaggregated before centrifugation to increase silt/clay ratio. The preparation was then filtered using a vacuum pump which concentrated the calcareous nannofossils to obtain clean samples. The method complete description is described in Lancis et al. (2023).

3. Biostratigraphy and biochronology

The calcareous nannofossil biostratigraphy at Hole 999A has been previously studied by Kameo and Bralower (2000) and Buitrago-Reina et al. (2010). In addition, events were compared with ages obtained by other authors for different points and basins (Raffi et al., 2006; Gradstein et al., 2012; Raffi et al., 2020) (Table 1 and Fig. 2). Site age calibration was conducted by means of a diagram of the orbitally tuned isotope

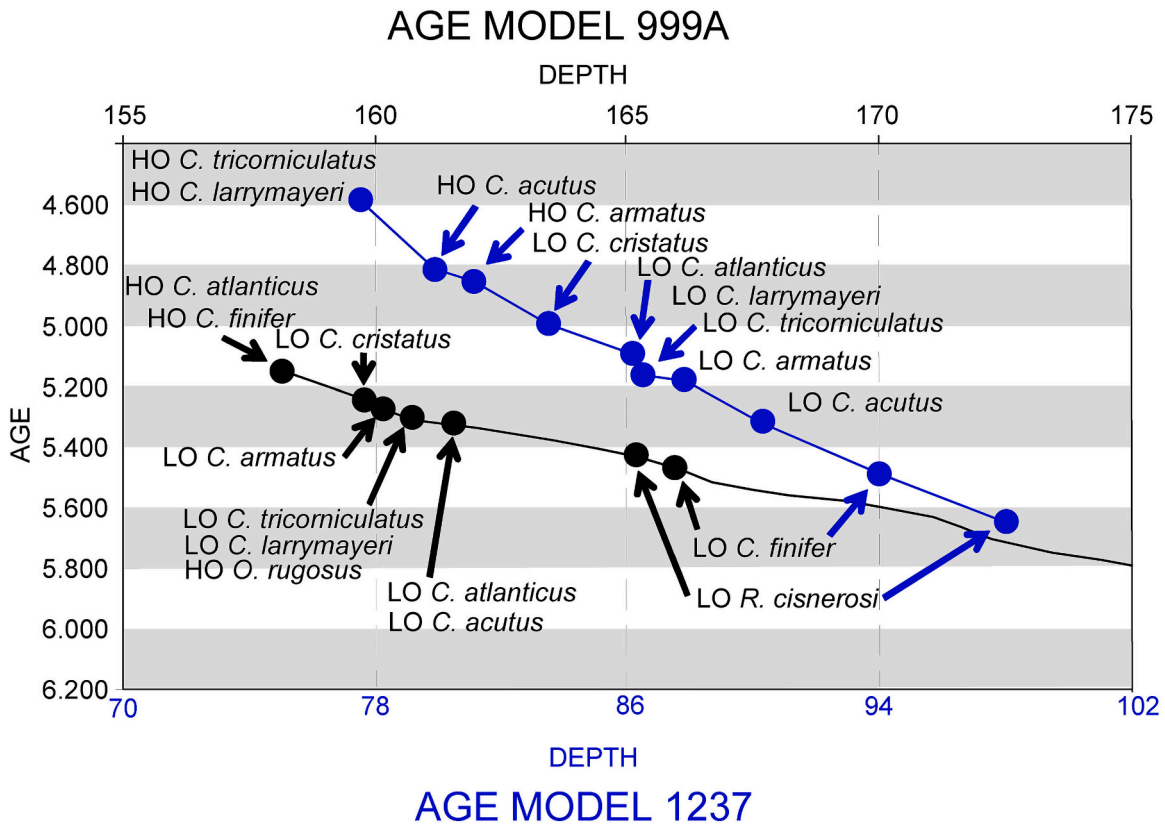

Fig. 2. Age model by orbital cyclicity of Hole 999A (black) after Bickert et al. (2004) and Haug et al. (2001) and composite age model of Site 1237 (blue) after Mix et al. (2003) showing the corrected depth (m) versus Age (Ma) from 6.2 to 4.5 Ma. Nannofossil events have been placed on it. (For interpretation of the references to colour in this figure legend, the reader is referred to the web version of this article.)

Table 2
Nannofossil events of Site 1237 composite used for age model calibration of Fig. 2.

Event	Core-section-CM	Mcd	Cmcd	AGE Ma Tiedemann et al. (2007)	AGE Ma (proposed 999A)
HO *C. larrymayeri*	1237B-9H-3W-75: **1237B-9H-4W-75**	83.14–**84.64**	75.93–**77.30**	4.661–**4.592**	
HO *C. tricorniculatus*					
HO *C. acutus*	1237B 9H-5W-75: **1237B 9H-6W-75**	86.15–**87.65**	78.53–**80.01**	4.726–**4.803**	
HO *C. armatus*	1237B-9H-6W-75: **1237B-9H-7W-45**	87.65–**88.87**	80.01–**81.12**	4.803–**4.865**	
LO *C. cristatus*	**1237B-10H-1W-75**: 1237B-10H-2W-75	**91.47**–93.02	**83.54**–84.96	**4.981**–5.042	**5.257**–5.260
LO *C. atlanticus*	**1237B-10H-2W-75**: 1237B-10H-3W-75	**93.02**–94.53	**84.96**–86.34	**5.042**–5.117	**5.322**–5.335
LO *C. larrymayeri*	**1237B-10H-3W-75**: 1237B-10H-4W-75	**94.53**–96.03	**86.34**–87.71	**5.117**–5.184	**5.299**–5.301
LO *C. tricorniculatus*	**1237D-6H-5W-124:** 1237B-10H-4W-75	**94.65** (1237D)–96.03	**86.45**–87.71	**5.174**–5.184	**5.299**–5.301
LO *C. armatus*	**1237B-10H-4W-75:** 1237B-10H-5W-75	**96.03**–97.53	**87.71**–89.19	**5.184**–5.251	**5.283**–5.299
LO *C. acutus*	**1237B-10H-6W-75**: 1237B-10H-7W-40	**99.04**–100.20	**90.67**–91.76	**5.301**–5.354	**5.322**–5.335
LO *C. finifer*	**1237B-11H-2W-75**: 1237B-11H-3W-75	**102.93**–104.94	**94.01**–95.84	**5.484**–5.539	**5.472**–5.523
LO *R. cisnerosi*	**1237B-11H-5W-75** 1237B-11H-6W-75	**107.46**–108.97	**98.14**–99.52	**5.643**–5.764	**5.472**–5.523

Mcd: metres composite depth of boreholes 1237B and 1237D, Cmcd: composite meters common depth of composite 1237. Age (Ma) from Tiedemann et al. (2007) calibration. Age (Ma) proposed from Hole 999A study. Event samples are indicated in bold font and the lower/upper samples in the LO/HO. Samples metres corrected depth (mcd) and the early/late calibrated ages are also shown.

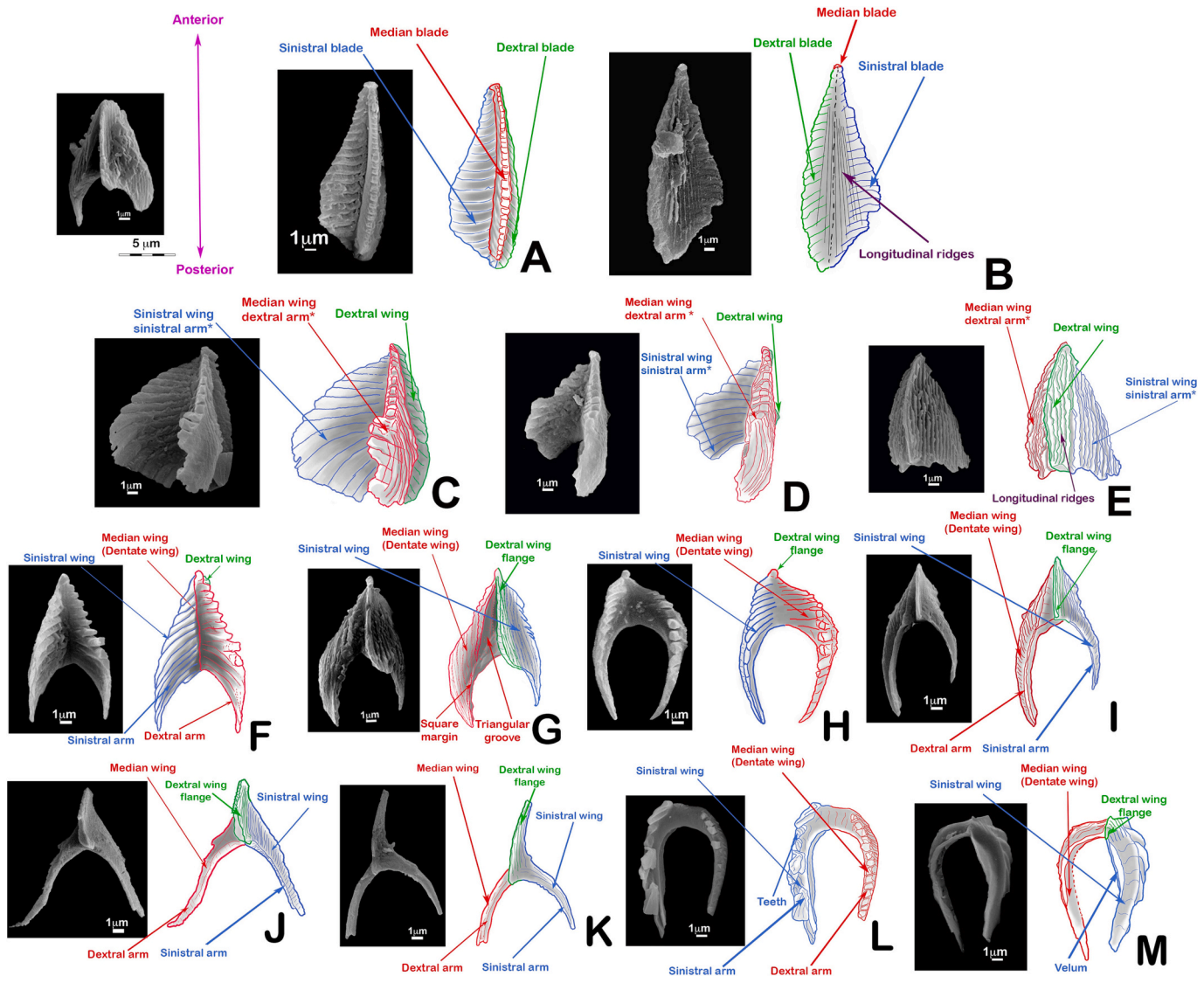

Fig. 3. Terminology used in this work. A: Top view *Orthorhabdus rugosus*; B: Bottom view *Orthorhabdus rugosus*; C and D: Top view *Ceratolithus finifer* *proto-arm; E: Bottom view *Ceratolithus finifer* *proto-arm; F: Top view *Ceratolithus acutus*; G: Bottom view *Ceratolithus acutus*; H: Top view *Ceratolithus armatus*; I: Bottom view *Ceratolithus armatus*; J and K: Bottom view *Ceratolithus larrymayeri*; L: Top view *Ceratolithus cristatus*; and M: Bottom view *Ceratolithus cristatus*.

record obtained with epibenthic foraminifera $\delta^{18}O$ and $\delta^{13}C$ (Bickert et al., 2004) from core 18 (>159.60 mcd) and down, and for the upper ones (17 and up), Haug and Tiedemann (1998) and Haug et al. (2001) calibration was used. Haug and Tiedemann (1998) and Haug et al. (2001) 17-core bottom part calibration does not match with Bickert et al. (2004) upper 18-core because of using two different timescales, Shackleton et al. (1995) for Haug and Tiedemann (1998)/ Haug et al. (2001), and Shackleton and Crowhurst (1997) for Bickert et al. (2004). The most recent one (Bickert et al., 2004) has been used to tie the bottom 17-core age (samples 17H-5 W-80 and 17H-6 W-90) of Haug and Tiedemann (1998)/ Haug et al. (2001).

Calcareous nannofossil biostratigraphy and biochronology (magnetostratigraphy, geochemistry, and isotopes) at Site 1237 have previously been studied by Mix et al. (2003). The site has three holes, 1237B, C and D, all integrated in the 1237 composite. The 1237A was not recovered (Mix et al., 2003). The tuned ages of the site magnetic reversals between 6 and 2.1 Ma were obtained by Tiedemann et al. (2007) but with an adjustment for the C3r (Gilbert)/C3n.4n (Thvera) inversion (5.235 Ma, GTS2020 Raffi et al., 2020) between 96.64 and 98.00 m in Hole 1237B. This variable interval for the tie point condition the calibration of the Messinian/Pliocene boundary events. Ages of the >5 Ma-datum biohorizons do not coincide with Hole 999A. Successive stratigraphic events are clear but the palaeomagnetic calibration of Tiedemann et al. (2007) is not consistent with our 999A bioevents (Table 1 and Fig. 2). Events used in this work were calibrated with the 999A borehole (Table 1), except for the highest occurrence (HO) of *C. armatus*, *C. acutus*, *C. tricorniculatus,* and *C. larrymayeri* which were calibrated with the 1237 composite (Table 2). However, they seem to be younger than expected when compared with the 999A data.

4. Morphology of ortholiths and ceratoliths

Specific terminology for the asymmetrical horseshoe-shaped form of ceratoliths was first established by Kamptner (1954), see also Gartner and Bukry (1975), Perch-Nielsen (1985), Aubry (1988), and Young et al. (1997). In a previous study, Lancis et al. (2022) revised the terminology to include the ortholiths (Fig. 3A–B). Ortholiths are elongate nannoltihs with a Y-shaped cross-section (Fig. 4). The entire nannolith behaves as a single crystal-unit in cross-polarised light but morphologically it can be described as being formed of three blades. In well-preserved samples

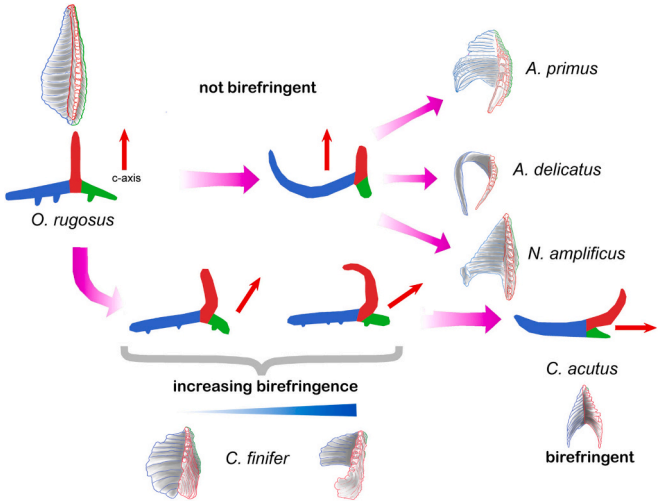

Fig. 4. Development of birefringence in the family Ceratolithaceae. Upper part, the first variability interval when *A. primus*, *A. delicatus,* and *N. amplificus* evolved from *O. rugosus*. As the median wing (in red) does not change its orientation, remaining perpendicular to the most stable position, pointing upwards, those species do not show birefringence. The lower part shows the *O. rugosus* second variability interval when *Ceratolithus* developed. The early forms, *Ceratolithus finifer,* show low birefringence as the c-axis/median wing (in red) incline towards the dextral wing (in green). In the later morphotypes the c-axis/median wing rotates, tilting the nannolith most stable position to the right, and so showing moderate to high birefringence. Finally, when the lath-end of the sinistral wing (in blue) of *C. acutus* rotates upwards, the nannolith most stable position tilts further to the right orienting the c-axis parallel to it, producing the high birefringence characteristic of *Ceratolithus*. (For interpretation of the references to colour in this figure legend, the reader is referred to the web version of this article.)

each blade can be seen to have a feather-like structure being formed of closely appressed rods running perpendicular to the length of the nannolith. Both ends of the nannolith are pointed but one end is consistently more sharply pointed, Lancis et al. (2022) designated this the anterior end, and the more bluntly pointed end the posterior end. The two broader blades of *O. rugosus*, lie nearly in the same plane, whilst the narrower median blade is oriented perpendicular to them. The most stable position for the nannolith is with median blade pointing up and we designate this the top surface. Having designated a top surface and anterior end, the two lateral blades can be distinguished as left/sinistral and right/dextral (Fig. 3). Orientations are directly comparable to the generally adopted orientations for ceratoliths (see Fig. 3). In the figures, the sinistral blade is shown in blue, the dextral blade in green and the median blade in red (Fig. 3A). This view is the top view, and bottom view is shown when median blade faces down, the nannolith bottom surface (Fig. 3B).

Fig. 3C-E shows *C. finifer* wings (triangular but asymmetric projectile-shaped) terminology following the same criteria as used for *O. rugosus* blades. *C. finifer* was previously described as a *Triquetrorhabdulus* species (Theodoridis, 1984) and it is included in the *Ceratolithus* in the present study (see Section 5). The nannolith preferred orientation observed in the PM is the more stable position with median blade (red in figures) in upright position (top). Pointed ceratolith can be oriented with acute portion drawn up (anterior portion). *Ceratolithus finifer* shows a sinistral (blue) wing made of parallel laths approximately 90° with respect to the wing joining margin, with their posterior half lath-ends trending towards the posterior portion, the not well-developed sinistral arm. Median (dentate) wing (red) was also made of robust laths and typically ended in a robust crenelated structure (Fig. 3C) is the not well-developed dextral arm, and the reduced dextral wing (green) had parallel laths at a 120-degrees angle with respect to median (dentate) wing. Dextral, sinistral, and median wings usually have numerous longitudinal ridges in bottom view. The same terminology, orientation, and colours have been used for *C. acutus* (Fig. 3F-G), *C. armatus* (Fig. 3H-I) and *C. larrymayeri* (Fig. 3J-K). In *C. acutus* (Fig. 3F-G) sinistral wing in top view is bent upward, acquiring a concave shape, forming the shorter left arm (blue). Median wing (red) forms the right arm. Both arms were wide, concave, generally short, pointed, and of similar size. *C. armatus* (Fig. 3H-I) has a triangular shape with arms longer than the arc (the anterior horseshoe closed end). Arms are narrow, pointed, and grooved on the inside margin, with a flange in the right arm in bottom view. Dextral wing is reduced to a flange and median wing has a triangular grove (Fig. 3G) and a square margin. *Ceratolithus larrymayeri* (Fig. 3J-K) had a stylised wish-bone shape with a thin apical spine of variable length. The long and narrow arms diverged and twisted at various angles.

Dextral wing was reduced in the three species, remaining as a flange at the junction of the three wings seen in bottom view (Fig. 3G-I-J-K). Two wings, sinistral and median, become the arms of the horseshoe. Pointed arm-end is the posterior portion and the opposite, the arc (also the horseshoe closed end), anterior portion.

Finally, median wing (red) and sinistral wing (blue) of *C. cristatus* were elongated and stylised (Fig. 3L-M). Sinistral wing (blue, also the right arm) has an irregular wavy edge as laths extend and form a corrugated surface. Late specimens show teeth of remarkable size, while others have the free surface of the former laths welded together, making it smooth with the appearance of a wavy veil (velum). Some forms developed a slight inner arch groove. Median wing (red, left arm) resembles a dentate keel with elongated teeth in top view. Owing to its fragility, the margin may be broken (Fig. 3L). In recent forms, median wing (left arm) can be of a considerable size. Ceratolith dextral wing (green) was kept as a reduced flange, seen in bottom view.

Archontikis and Young (2020) concluded that two *Ceratolithus* species occur in modern oceans, *C. cristatus* and *C. nishidae*. Recently Young (2023) considered the last one as a junior synonym of *C. vidalii,* that should be used instead.

5. *Orthorhabdus rugosus* ancestor of *Ceratolithus finifer*

Orthorhabdus rugosus shows increased morphological variability during two time-intervals (Lancis et al., 2022): 1) The latest Tortonian to the Early Messinian, and 2) latest Messinian to Early Pliocene. The first is coincident with the appearance of the *Amaurolithus* and *Nicklithus* genera between 7.36 Ma and 6.91 Ma and discussed in Lancis et al. (2022). The second coincides with the appearance of the genus *Ceratolithus* around 5.36 Ma (Raffi et al., 2020).

Lancis et al. (2022) considered that *O. extensus and O. striatus are morphovariants of O. rugosus* distinguished respectively by a more extended sinistral blade and by development of secondary ridges. During the first variability interval, the sinistral and dextral blades changed significantly in shape (blue and green Fig. 3A-B), becoming the sinistral and dextral arms of the *Amaurolithus/Nicklithus* and median blade remained without major changes (dextral arm composed by the dextral and median blades). The three genera have c-axis perpendicular to the ortholith or ceratolith in the most stable orientation (Fig. 4). This c-axis seems to coincide with median blade/wing. As this blade/wing almost remains unchanged pointing upwards in this time-interval, nannoliths do not show birefringence.

However, in the second *O. rugosus* variability interval, latest Messinian to Early Pliocene, changes fundamentally affect the median (dentate) (red in Fig. 3A and B) and sinistral (blue in Fig. 3A and B) blades, with an elongation of both blades forming the *Ceratolithus* dextral and sinistral arms. Concurrently, the dextral blade (green) is reduced until it becomes a flange (Fig. 3G). This process changed the most stable orientation, tilting the nannolith to the dextral wing, and also the c-axis. So, the nannolith showed low to high birefringence (Fig. 4), as the c-axis tilts towards the dextral wing.

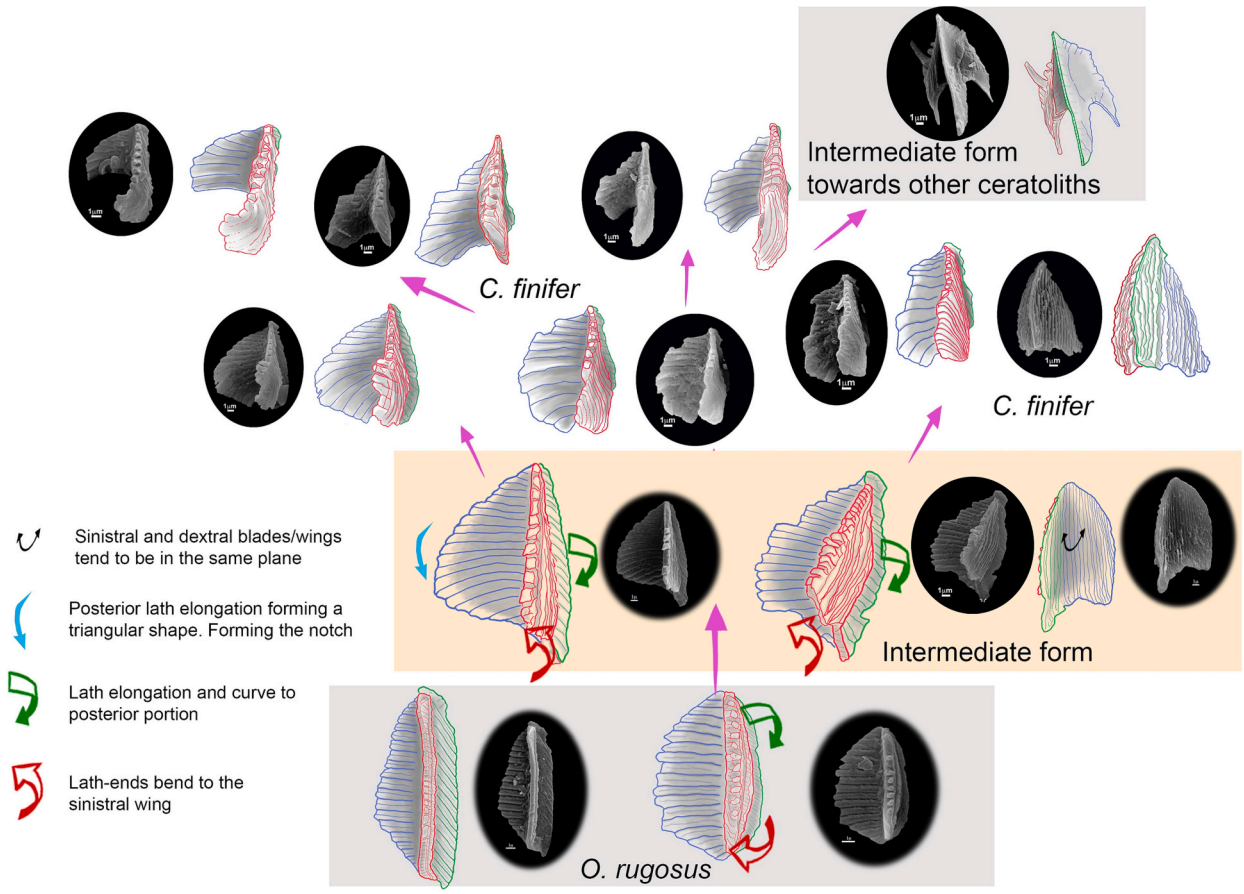

Fig. 5. *Ceratolithus*-branch evolution: *C. finifer* from *O. rugosus*. The SEM pictures have been used to make schematic drawings. Sinistral blade, (*O. rugosus*), or wing (*C. finifer*) blue; Dextral blade, (*O. rugosus*) or wing (*C. finifer*) green; Median blade (*O. rugosus*) increases its size and turns to sinistral blade forming the dextral proto-arm (*C. finifer*, red). Intermediate form sinistral and median blades increase their size. Sinistral blade stays in the same plane. The arrow colour indicates blade/wing affected. (For interpretation of the references to colour in this figure legend, the reader is referred to the web version of this article.)

Morphotypes in which only the sinistral blade extends laterally to become roughly triangular, have been named *Triquetrorhabdulus extensus* (Theodoridis, 1984) Similarly, morphotypes with a very large and crescent-shaped fin-like apical blade, have been named *T. finifer* (Theodoridis, 1984). *Triquetrorhabdulus finifer* was found by Theodoridis (1984) at the Pliocene bottom, together with the first *C. acutus*. Also, it was considered non-birefringent in the most common orientation.

Studied samples of Sites 999 and 1237 indicate that *T. finifer* of Theodoridis (1984) is the first species of the *Ceratolithus* lineage. Theodoridis (1984) defined *T. finifer* as non-birefringent forms, but in the studied samples, *C. finifer* showed low to moderate birefringence. Nevertheless *O. rugosus* stable position led to consistent non-birefringence in PM while it also can lie with the median blade pointing down and, in this orientation, it is slightly tilted and so shows low birefringence. (see fig. 8.5 of Young, 1998). However, in *C. finifer* case, they do not possess a single most stable position due to their shape (Fig. 3C, D and F). Because *C. finifer* can rest in various different orientations, these nannoliths may exhibit low or high birefringence, or even non-birefringence, when viewed under a polarising microscope. The median (dentate) wing is usually brighter. As it usually shows birefringence we believe it should be included in the *Ceratolithus* genera and named *Ceratolithus finifer* n. comb.

The older *C. finifer* forms with many laths in the sinistral wing and the upward-extended median wing show, in top view, low birefringence (Fig. 4) whilst later forms with an extended median wing the lath-ends are bent towards the sinistral wing, forming both the right and left proto-arms, show moderate to high birefringence (Fig. 4). Evolution changes the c-axis orientation relative to the most stable layout.

The *O. rugosus*-*C. finifer* intermediate forms show progressive increase of the median blade size, although it was straight (Figs. 6G-M and 7). Its median wing shows a gradual tendency to increase in size and thickness (Fig. 7G-O) and curve its posterior half-end to sinistral blade (Figs. 6N-O, 7G-O and 8A-G). The posterior margin-end separates from sinistral wing, elongates, and forms the arch. Dextral wings size decreased. Within the *C. finifer* variability, ancestral forms intermediate towards future *Ceratolithus*, as *C. acutus* (Fig. 7M-O), *C. armatus* (Fig. 8L-O), and *C. larrymayeri* can be found (Fig. 9).

The more recent forms, coincident with *C. acutus* appearance, show a reduction in the number of laths and in the size of the anterior laths, elongation of the posterior lath and its twirl forming an oval notch as the arch precursor. Then median wing (red) laths tend to weld, thicken (Fig. 8H-O), and turn towards the sinistral blade in its posterior half, separating from it, producing the dextral arm (Fig. 5).

The proposed criteria to differentiate between *C. finifer* and early forms of *C. acutus,* is that the sinistral wing curves the lath-ends to the upper view in *C. acutus*. The nannoliths shape became a symmetric arrow and concave in top view, showing high birefringence.

The last record (HO) of *O. rugosus* is in sample 999A 18H-1W-145, which corresponds to 5.299 Ma, compared with the lowest occurrence (LO) of *C. finifer* in sample 999A 18H-5W-110, 5.472 Ma, and its HO in sample 999A 17H-6W-90, 5.173 Ma. Within this time range, it became feasible to regard *C. finifer* as a distinct species with its unique characteristics.

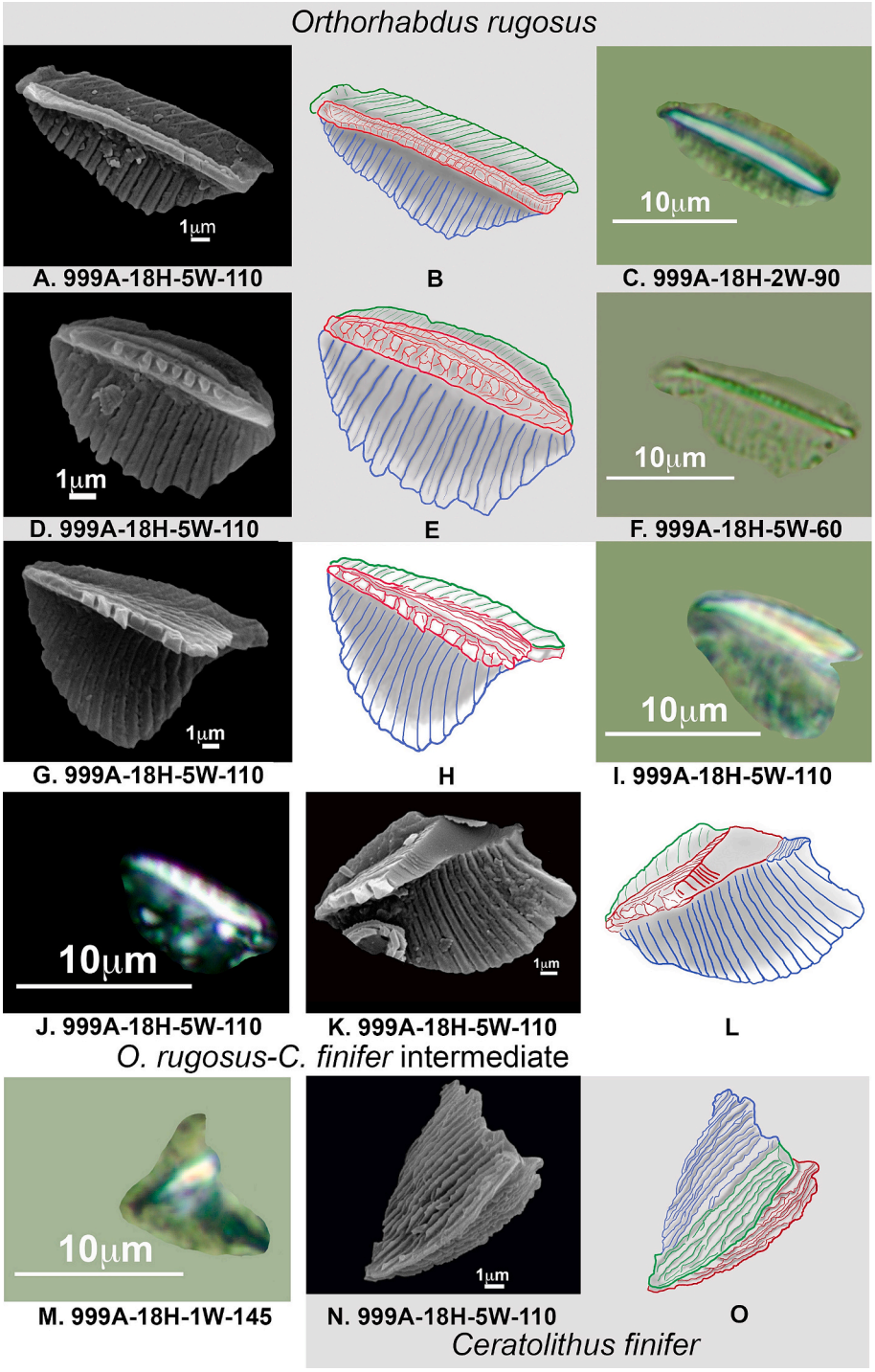

Fig. 6. *Orthorhabdus rugosus, O. rugosus-C. finifer* intermediate and *C. finifer* morphological variability. A: *O. rugosus* top view SEM; B: Drawing after the picture shown in A; C: *O. rugosus* in plane polarised light (ppl) with phase contrast equivalent to A; D, G and K: *O. rugosus-C. finifer* Intermediate form top view SEM; E, H and L: Drawings after the pictures; F, I and M: Pictures from ppl equivalents to D, G and K images respectively, I and M with phase contrast; J: Pictures from cross-polarised light (xpl) equivalents to G; N and O: *C. finifer* SEM in bottom view.

6. Origin of *Ceratolithus acutus, C. armatus* and *C. larrymayeri*

Ceratolithus acutus, C. armatus and *C. larrymayeri* evolved from *C. finifer* (Fig. 9). By analysing and comparing the homologies between species, it becomes possible to trace the series of morphological changes that lead to their emergence from their common ancestor.

The starting point is *C. finifer* showing intermediate characteristics (Fig. 10A–B) with all of them. The first to evolve was *Ceratolithus acutus*, acquiring an arrowhead shape with the sinistral wing curved towards the observer. The sinistral wing (blue) became more pointed as a consequence of curving and elongation of its laths (Fig. 3F-G). The posterior edge, inside the arch, became smoothly rounded, in contrast to the irregular anterior/outer edge. The dextral wing (green) was reduced to a flange. A characteristic crenulated margin developed along the anterior edge of the median wing. The inside arch developed a square margin and a triangular-shaped surface plane parallel to median-dextral

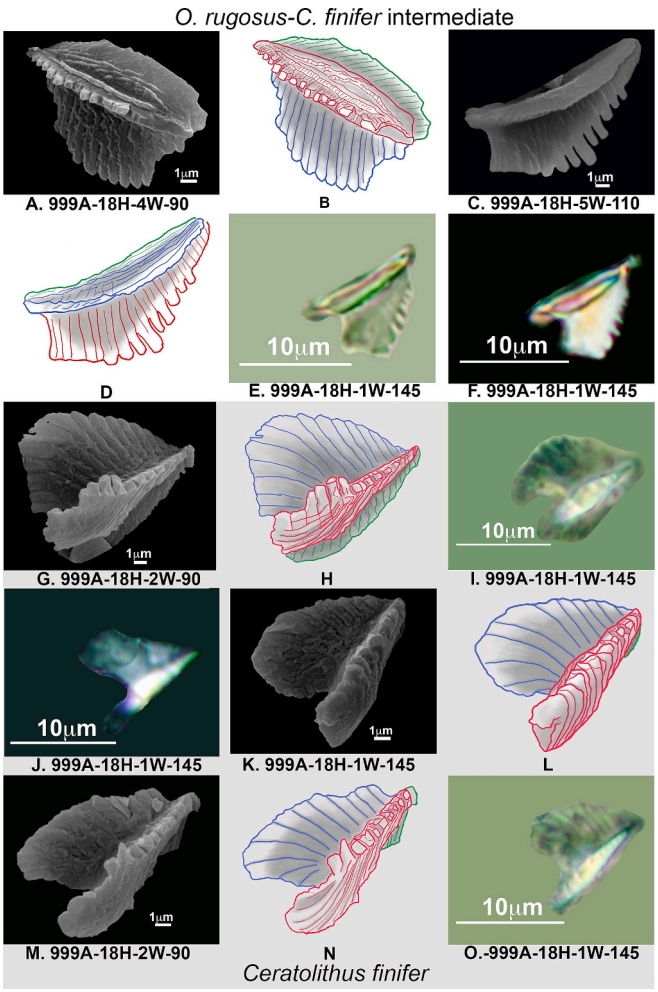

Fig. 7. *Orthorhabdus rugosus- C. finifer* intermediate and *C. finifer* morphological variability. A and C: *O. rugosus-C. finifer* intermediate SEM, A in upper view and C Lateral vision; B and D: Drawings after the pictures; E: *O. rugosus-C. finifer* intermediate form ppl; F: *O. rugosus-C. finifer* intermediate xpl, high birefringence; G, K and M: *C. finifer* SEM top view; H, L and N: Drawings after the pictures; I and O: *C. finifer* ppl equivalents; J: *C. finifer* xpl low birefringence equivalents to G.

wing join, the triangular grove (Fig. 3G), seen in bottom view, along dextral arm. *C. acutus* has a triangular concave shape in top view, with the horseshoe apical region (anterior) longer than the arms (Fig. 3F-G).

Ceratolithus armatus and *C. larrymayeri* also evolve from the intermediate species *C. finifer* (Fig. 10A-B) with shorter right arm, a triangular sinistral wing (proto-arm), an elongated median wing (dextral arm), having concave shape in top view and a flange in bottom view. However, the set of changes in the two descendants are different, which is interpreted as reflecting phylogenetic branching starting from the same ancestral species (*C. finifer*).

Initially, the *C. finifer* ancestor of the *C. larrymayeri-C. armatus* lineage has a wide arch and the dextral arm larger than the apical region. The intermediate form from which both species could have developed is shown in Figs. 9 and 11A-C.

The changes to develop *C. armatus* can be described as follows: The sinistral wing (sinistral arm) extends to become nearly as long as the dextral arm. The arms are longer than the triangular apical region, and the arms tips converge (Fig. 9), resulting in a clearer horseshoe shape. *Ceratolithus larrymayeri* evolved differently, initially the arms elongated, to an equal extent, were reduced in thickness and diverged. In addition, the sinistral arm flattens. Finally, the apex is prolonged producing the characteristic chicken wish-bone shape (Fig. 9).

Typically, in the bottom view all of these species show parallel, or slightly oblique, longitudinal ridges parallel to the length of (Fig. 3I 10A, 10J, 10L, 10N, and 11F). These ceratoliths have an arrowhead-like form and show maximum birefringence when oriented at 45° to the polarisation direction.

The sequence of small changes accumulated in different phyletic lines, was marked by gradual but obviously not monotonic, replacement of the old morphotype by the new morphotype and as in the *C. finifer* evolution, there was no sustained change in one direction and reversals of direction are common, as occurs in planktonic foraminifera (Malmgren et al., 1983). The Figs. 10, 11, and 12 show the variability in the three ceratoliths observed at ODP Sites 999 and 1237.

In the nannotax 3.0 database the *Ceratolithus* genus is composed by the genera: *C. apiculus, C. armatus, C. larrymayeri, C. atlanticus, C. cristatus, C. vidalii,* and *C. separatus* (Young et al., 2023a). The first three can be included in this evolution branch. Young (1998) considered *C. armatus* and *C. acutus* to be synonyms (Young et al., 2023b). As mentioned above our observations suggest that the two ceratoliths evolve separately from *C. finifer*, and so should be considered as two different species. Blair et al. (2017) subdivide this group into 4 species *C. acutus, C. armatus, C. cornulum,* and *C. apiculus*, mostly for biostratigraphic reasons. *Ceratolithus cornulum* is a form with long curved arms and smoothly curved apical region (Blair et al., 2017). Here these morphotypes are included in *C. armatus*, examples are shown in Fig. 12E-G and L-O. Finally, *C. apiculus* was proposed by De Kaenel et al. (2017) and was documented as restricted to the NN12 by Blair et al. (2017). It has short arms, and a highly pointed apical region. Some of the specimens figured in Blair et al. (2017 pl. 10 12-17) can be included in *C. acutus* (similar ones are shown here in Fig. 10M-O). Their other specimens (Blair et al., 2017 pl 10 06–11), with a shorter sinistral arm, appear to be intermediate forms to *C. armatus* and *C. larrymayeri* (similar to our Fig. 10A-C).

The LO of *C. acutus* in our studied boreholes is in sample 999A 18H-2W-90, 5.322 Ma, and HO of *C. acutus* 1237B 9H-6W-75, 4.803 Ma; LO of *C. armatus* is in sample 999A-18H-1W-90, 5.283 Ma, and HO in sample 1237B-9H-7W-45, 4.865 Ma, and *C. larrymayeri* LO is in sample 999A-18H-1W-145, 5.299 Ma, and HO sample 1237B-9H-4 W-75, 4.592 Ma.

7. Origin of *Ceratolithus cristatus*

Ceratolithus cristatus Kamptner, 1950 *emend.* Bukry and Bramlette, 1968 is similar to *C. armatus* but differs in lacking the "latter's pronounced triangular apical spine". Gartner and Bukry (1975) regarded it as a Pleistocene-Holocene species that evolved from Pliocene *Ceratolithus rugosus*. However, they point out that it is difficult to specify the moment of its appearance, although they place it at the level of the Pliocene-Pleistocene boundary. Bergen (1984) and Young (1998) observed its first occurrence (FO) at the base of the NN13 zone (5.1 Ma, in the Zanclean stage, Pliocene) and considered *C. rugosus* to be a junior synonym of *C. cristatus*, based on overgrown specimens. Young (1998) also regarded *C. separatus, C. simplex,* and *C. telesmus* as synonyms of *C. cristatus*. Blair et al. (2017) place its appearance at 5.059 Ma. Recently, Archontikis and Young (2020), argued that two *Ceratolithus* species occur in modern ocean, *C. cristatus* and *C. vidalii* (Young, 2023).

In the borehole samples studied, no overgrowth on any coccolith specimens have been observed in Hole 999A, and *C. rugosus* morphologies were not seen, but at Site 1237 (in the interval: 6–4 Ma), some coccoliths show overgrowth and some *C. rugosus* morphotypes were seen. These specimens have been included in *C. cristatus* following Young et al. (2023d). *I. e.* we considered them to be overgrown *C. cristatus* specimens. The first specimens of *C. cristatus* observed are

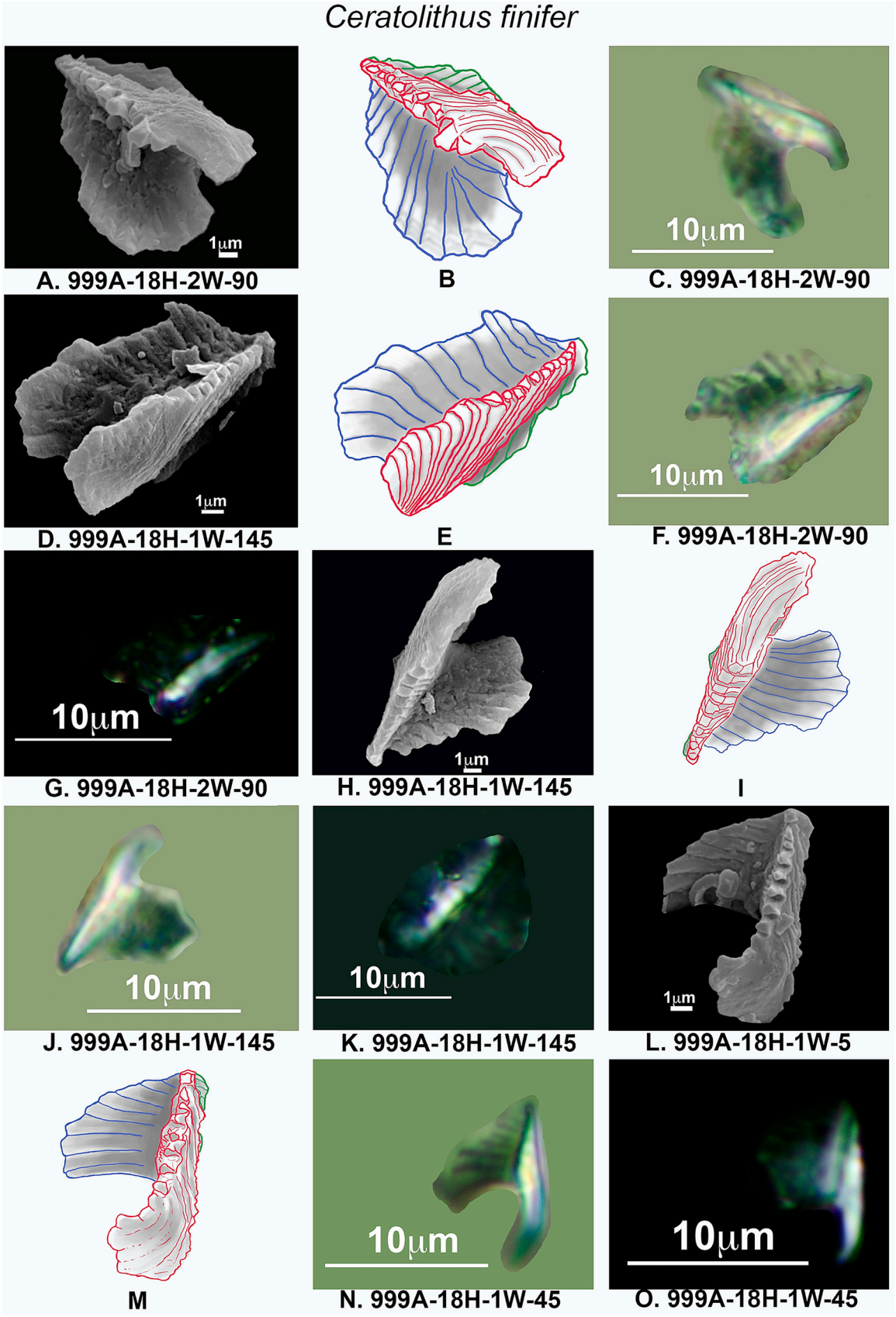

Fig. 8. *Ceratolithus finifer* morphological variability. A, D, H and L: *C. finifer* SEM top view; B, E, I and M: Drawings after the pictures; C, F, J and N: *C. finifer* ppl equivalents; G, K and O: *C. finifer* from xpl low birefringence.

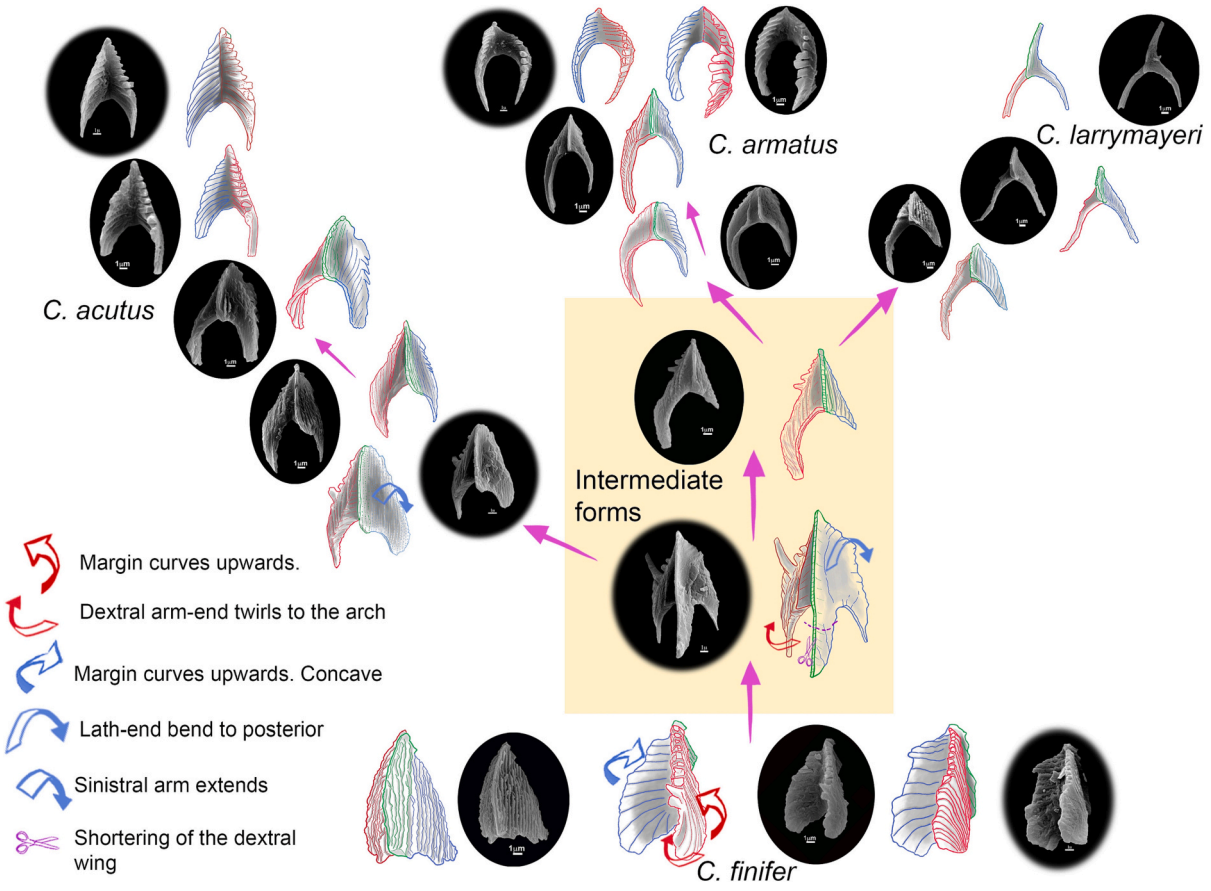

Fig. 9. Origin of *C. acutus, C. armatus,* and *C. larrymayeri* from *C. finifer*. The SEM pictures have been used to make schematic drawings. Blue, sinistral wing; Green, dextral wing; Red, median wing. Arrows colours indicate the blade/wing affected. (For interpretation of the references to colour in this figure legend, the reader is referred to the web version of this article.)

closely related to *C. armatus* from which they differ almost exclusively because the former lack the pronounced triangular apical area.

Optically, *C. cristatus* is highly birefringent in the PM preferred orientation; it is brightest with arms at approximately 45° to the direction of polarisation and goes into extinction with the arms approximately parallel to the direction of polarisation (Gartner and Bukry, 1975).

Fig. 13 shows the changes producing *C. cristatus* from *C. armatus*. Both arms extend, the sinistral arm is almost straight, whilst the dextral arm curves, closing the horseshoe ends. The sinistral arm, in some modern forms, is covered by lamina formed by the extension of the straight edge covering lath (velum).

The first forms of *C. cristatus* (Fig. 14A-F) differ from *C. armatus* (Fig. 12E-G and L-O), because the former lacks a pronounced triangular apical spine. There is a tendency to increase ornamentation in the most evolved forms. Some *C. cristatus* specimens had sinistral arms with pronounced edges (Fig. 14M-O), or in both arms (Fig. 14C-D), named by Bukry (1979) as *C. separatus*, and elongation of delicate arms that curve together to almost touch (Fig. 14K-L) *C. cristatus* var. *telesmus*.

Studies of extant *Ceratolithus* (see Archontikis and Young, 2020 for references) have shown that there is alternation of a life cycle phase with ceratoliths surrounded by hoop coccoliths and an alternate phase covered by planoliths. These phases are inferred to probably be haploid and diploid respectively. The *coccolithomorpha*-type planoliths are associated with *cristatus/telesmus*-type ceratoliths, whereas the *vidallii*-type planoliths are associated with *rostratus*-type ceratoliths, thus allowing their division into two species, *C. cristatus* and *C. vidalii* (Fig. 14O), respectively (Archontikis and Young, 2020; Young, 2023).

The first appearance of *C. cristatus* is in sample 10H-1W-75 of site 1237B calibrated at 4.981 Ma and in sample 18H-1W-5 of site 999A at 5.257 Ma. In the first site, *C. cristatus* has overgrowth (*C. rugosus* morphotype) whilst in the second site, *C. cristatus* does not show any overgrowth. This species is distributed in recent oceanic basins.

8. Discussion

The genera *Amaurolithus* and *Nicklithus* appeared suddenly at different times during the Late Miocene (Raffi et al., 1998; Lancis et al., 2022); Nevertheless, *Ceratolithus* was also derived from *O. rugosus*, albeit the evolutionary paths vary among the different species.

The evolutionary changes producing *C. finifer* fit a model of phyletic gradualism while the pattern for *C. acutus, C. armatus* and *C. larrymayeri,* follows a punctuated gradualism model with lineage splitting (Malmgren et al., 1983; Fig. 15). The first *Ceratolithus*, *C. finifer*, showed great morphological diversity. A series of gradual modifications can be observed (Fig. 5), particularly affecting median blade/wing (red) derived from *O. rugosus* median blade (red). This trend led to the intermediate form *O. rugosus-C. finifer* and it was followed by a diversity of *C. finifer* forms. All of them showed birefringence in its most stable orientation. This is the reason we included this species in the genus

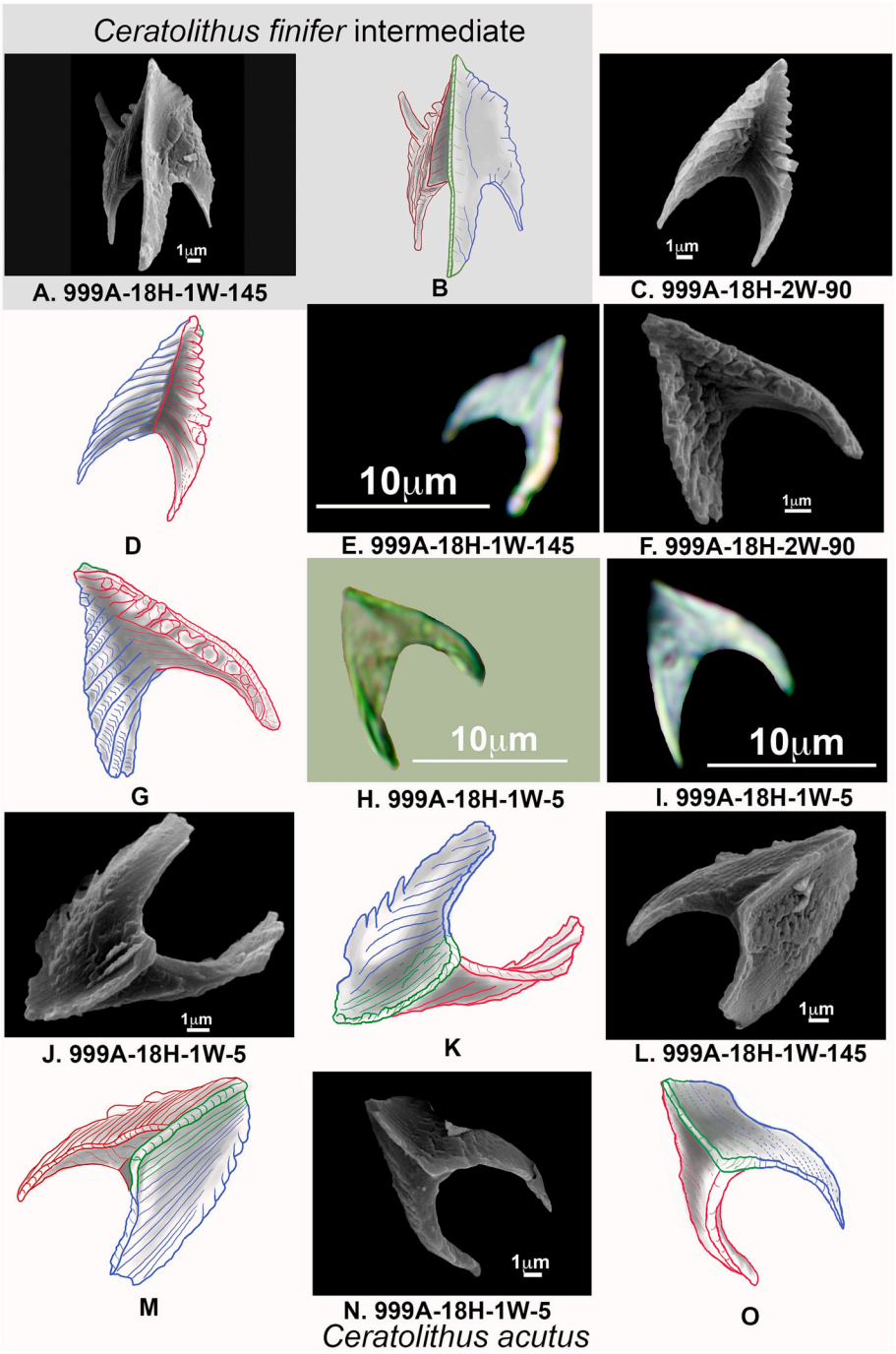

Fig. 10. *Ceratolithus acutus* morphological variability. A and B: *C. finifer* intermediate to other *Ceratolithus* sp. (See explanation in the text); C, F, J, L and N: *C. acutus* obtained by SEM; C and F top view; J, L and N bottom view; D, G, K, M and O: Drawings after the pictures; H: *C. acutus* obtained with the ppl equivalents to F; E and I: *C. acutus* from xpl equivalent to C, and F.

Ceratolithus and made it the first species of the genus. The transition was a gradual process, with irregular fluctuations in one predominating direction (Malmgren et al., 1983). This change may be attributed to random walks which may be indicative of random genetic drift or randomly changing selection (Raup and Crick, 1981).

As depicted in Fig. 15, *C. acutus, C. armatus,* and *C. larrymayeri* were derived from *C. finifer* by a punctuated gradualism model with lineage splitting (Malmgren et al., 1983). Despite the gradualistic pattern of evolution observed within each lineage (Fig. 8), leading to great morphological variability.

All species show significant variability due to small variations, typically spanning from older dominant robust forms to stylised forms with long arms while maintaining distinctive traits that define species. All of them have an arrowhead shape, more or less symmetric, and are highly birefringent, when the ceratolith plane lies perpendicular to the direction of illumination.

The last ceratolith in our study is *C. cristatus* (appearing at 5.257 Ma), which originated from *C. armatus* by a lineage splitting model. The morphological difference separating the initial *C. cristatus* from *C. armatus* is that the former lack a pronounced triangular apical region.

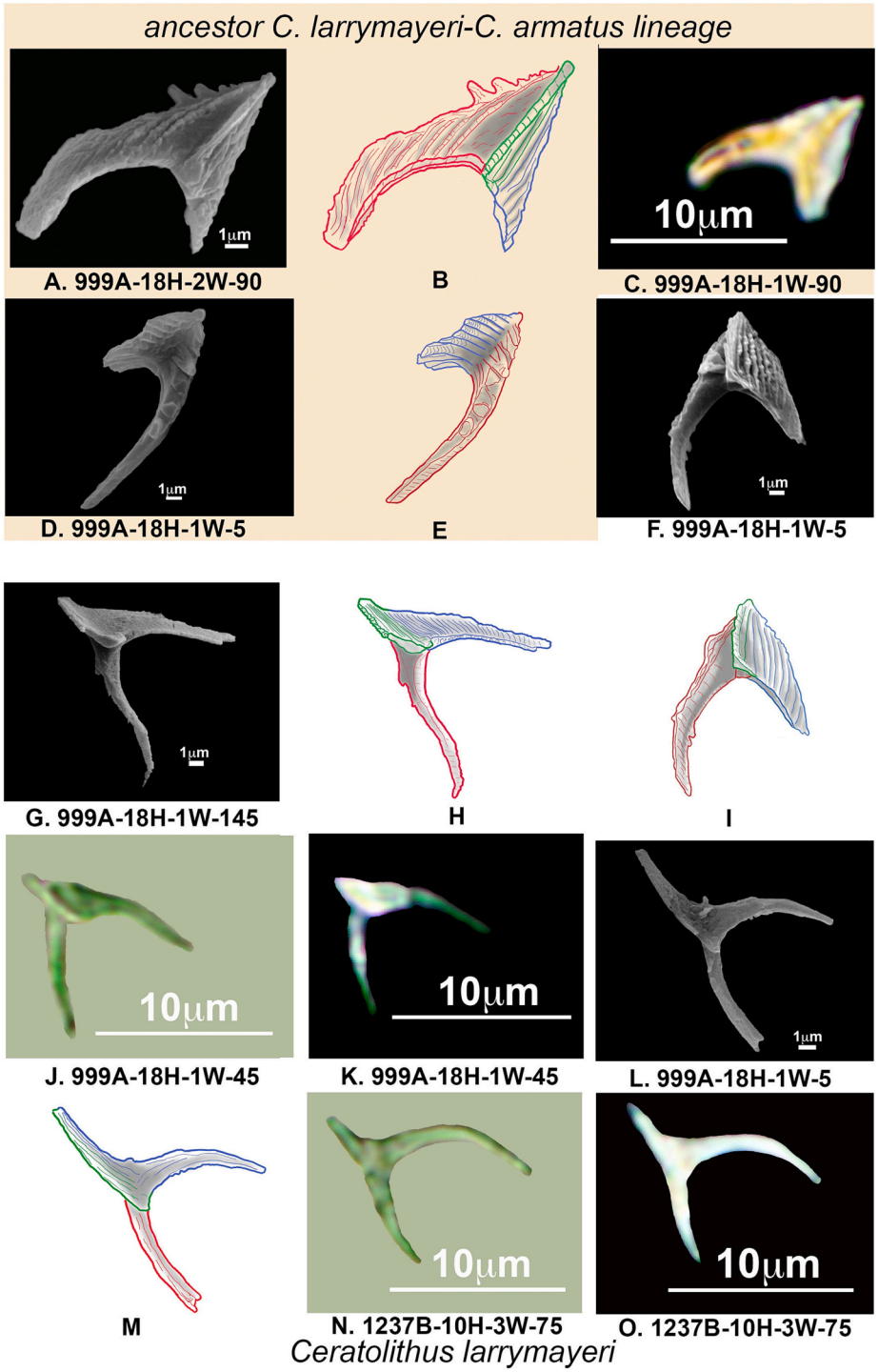

Fig. 11. *Ceratolithus larrymayery* morphological variability. A: Intermediate form, ancestor of *C. larrymayeri-C. armatus* lineage SEM; C: *C. larrymayeri-C. armatus* lineage intermediate, xpl equivalents to A and C; D: *C. larrymayeri-C. armatus* lineage intermediate SEM; B and E: Drawings after the pictures; F: *C. larrymayeri* initial form SEM; I: Drawing after the picture F; G and L: *C. larrymayeri* SEM; H and M: Drawings after the picture; J and N: *C. larrymayeri* from ppl equivalents to G and L respectively; K and O: *C. larrymayeri* xpl of J and N. D: top view; A, F, G and L: bottom view.

Over time, morphological variability is progressively accentuated, along with forms that remain practically identical to the initial ones, others have notable differences, but they always retain the basic characteristics of the species considered here within the variability range.

The *Ceratolithus* genus is composed in the nannotax 3.0 database of: *C. apiculus, C. armatus, C. larrymayeri, C. atlanticus, C. cristatus, C. vidalii,* and *C. separatus* (Young et al., 2023a). *Ceratolithus apiculus* is included in *C. acutus*, *C. armatus* is split into *C. acutus* and *C. armatus*, *C. separatus* is included in *C. cristatus*, and C. *larrymayeri* and *C. vidalii* are species separated. The only species not discussed here is *C. atlanticus,* which do not have the typical horseshoe shape and is also birefringent in its stable view. This ornate complex "ceratolith" with spines (Young et al., 2023c) evolve from morphotypes of *C. finifer*, also producing other birefringent forms as *C. tricorniculatus* and *C. bizzarus*. This will be described in a future work.

The time-interval range for *C. finifer* in ODP boreholes 999 and 1237,

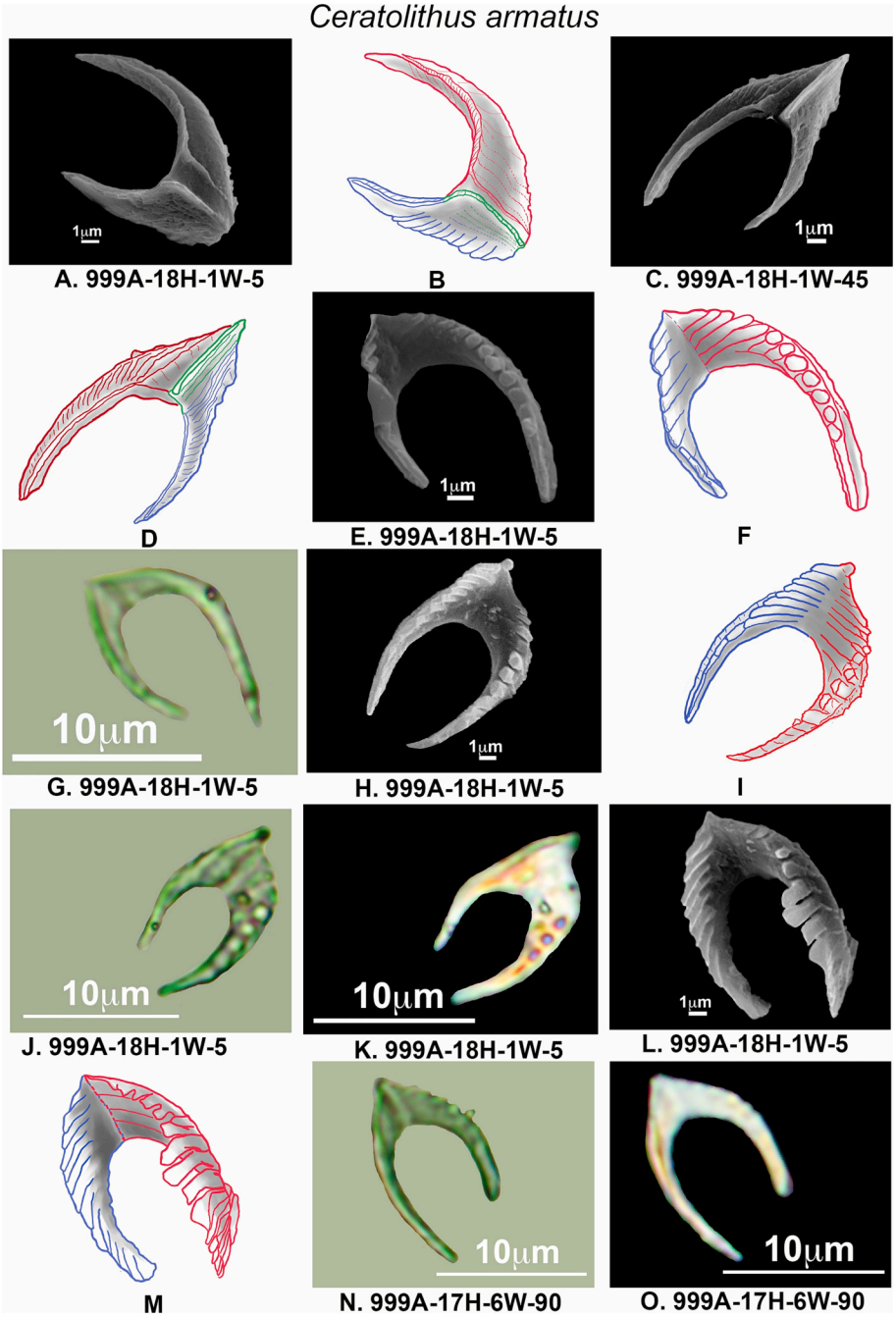

Fig. 12. *Ceratolithus armatus* morphological variability. A: *C. armatus* initial forms SEM; C, E, H and L: *C. armatus* SEM; A and C bottom view; E, H and L top view; B, D, F, I and M: Drawings after the picture; G, J and N: *C. armatus* from ppl equivalents to E, H and L; K and O: *C. armatus* xpl of H and L.

based on previous age calibrations (Haug and Tiedemann, 1998; Haug et al., 2001; Bickert et al., 2004; Tiedemann et al., 2007), was between 5.484 and 5.173 Ma, *C. acutus* 5.322–4.803 Ma, *C. armatus* 5.283–4.865 Ma, *C. larrymayeri* 5.299–4.592 Ma. The extinction of *O. rugosus* occurred at 5.299 Ma, and the appearance of *C. cristatus* at 5.257 Ma in our studied samples. The ages appear to be younger than expected, as the First Appearance Datum of *C. acutus* has been calibrated later than Messinian/Pliocene Boundary at 5.33 (Gradstein et al., 2012; Raffi et al., 2020).

Evolutionary change in microplankton can be driven by abiotic forces (Schmidt et al., 2004). During the Pliocene, changes affecting water circulation, biological productivity, and upwelling states occurred. According to Filippelli and Flores (2009), the Pliocene oceans, spanning from low to high latitudes, were characterised by temperatures ~3 °C higher than the current ocean temperatures (Haywood et al., 2000, 2009; Dowsett et al., 2009; Dowsett and Robinson, 2009; Naish et al., 2009), and the atmosphere had ~30% higher CO_2 concentrations than pre-industrial Holocene levels (Kürschner et al., 1996; Raymo et al., 1996). It appears that a "permanent" El Niño state prevailed in the Pacific Ocean (Ravelo et al., 2004; Wara et al., 2005; Dowsett et al., 2009), with a reduction in the east-west pressure gradient affecting wind regimes and heat distribution. This atmospheric state resulted in a

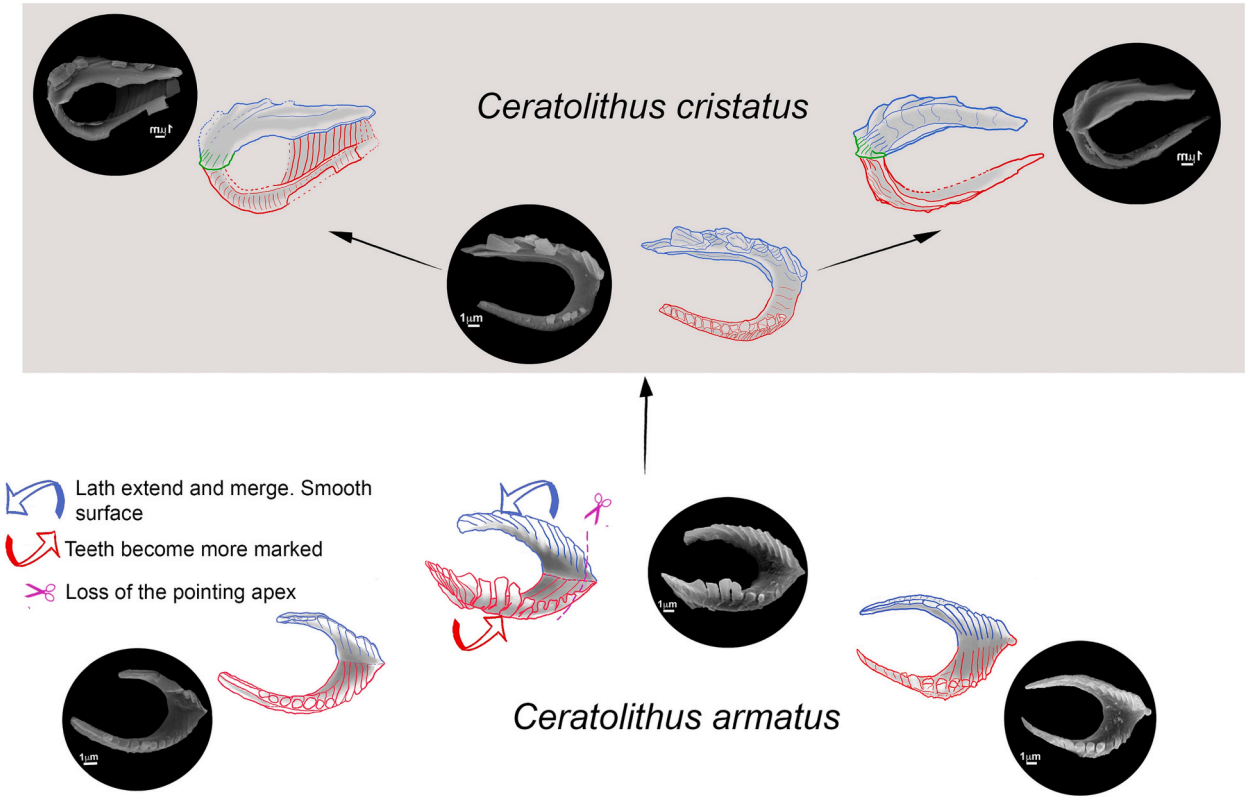

Fig. 13. Evolutionary origin of *Ceratolithus cristatus* (D—F) from *C. armatus* (A-C). Blue the sinistral wing; Green the dextral wing (flange); Red the median wing. (For interpretation of the references to colour in this figure legend, the reader is referred to the web version of this article.)

deepening of the thermocline and a reduction in upwelling intensity in the Pacific Ocean. In the North Atlantic Ocean, several authors (Raymo et al., 1996; Haywood et al., 2009; Dowsett et al., 2009) have suggested intensification of the thermohaline circulation, and consequently the Gulf Stream and North Atlantic currents, enhancing heat transport from the tropics and increasing North Atlantic temperatures.

These oceanic and atmospheric changes lead to a period of high instability, favouring the natural selection of some traits over others from the genetic background by causing a greater particularisation of the environmental conditions and, therefore, the genesis of new niches. During the short time interval between the first appearance of *C. finifer* (5.484 Ma in Hole 1237B) and the first appearance of *C. cristatus* (5.257 Ma), which is approximately 0.23 Ma, seven species of the Ceratolith branch (*C. finifer*, *C. acutus, C. armatus*, *C. larrymayeri, C. atlanticus*, *C. tricorniculatus*, and *C. cristatus*) appeared (Fig. 15). So, it may be that the period of high stress and changes in the oceans during the earliest Pliocene was the abiotic driver of *Ceratolithus* evolution.

Lancis et al. (2022) pointed out the relationship between the median blade/wings, in the three branches of ceratoliths (*Amaurolithus*, *Nicklithus* and *Ceratolithus*) and *O. rugosus*. In *C. finifer* the median wing was extended and rotated towards the sinistral. This caused the stable orientation of the nannolith to change and so it showed birefringence. In *C. acutus, C. armatus,* and *C. larrymayeri* the sinistral wing bent upward, and the dextral wing was reduced causing change in the nannolith stable position. Furthermore, the median wing locates to a most parallel position with respect to the slide preparation plane. All the changes may orientate the crystallographic c-axis sub-parallel to horseshoe stable plane, producing *Ceratolithus* high birefringence (Fig. 4).

9. Conclusions

The study of the sediments of the equatorial Pacific and Caribbean Sea ODP Sites 1237 and 999 during the time-interval between 6 and 4.5 Ma has permitted study of the *Ceratolithus* genus evolutionary origin and its diversification in species. Based on the observed morphological and structural features modifications in dated stratigraphic ODP-borehole sequences, we constructed lineages.

Ceratolithus lineage (5.484 Ma) was derived from *O. rugosus,* an ortholith with three blades (sinistral, median, and dextral), in some moment around the Messinian-Pliocene boundary. Major changes occurred in the sinistral and median blades of *O. rugosus* which will finally form the *Certatolithus*-horseshoe nannolith sinistral and dextral arms. Taxonomic description has been improved based on the evolutionary line. *Ceratolithus finifer* evolutionary changes produce a variation of its stable position, therefore showing birefringence in the PM preparation, thus, it has been included in the *Ceratolithus* genus, being the first species of the *Ceratolithus*-lineage.

Ceratolithus acutus, which displays high birefringence in its stable layout, was derived from *C. finifer*. Derived forms from *C. finifer,* also produced *C. armatus* and *C. larrymayeri*, which also showed high birefringence as commonly observed in the PM.

Finally, the loss of the two-arm union triangular shape due to the lack of the pointing end of *C. armatus* produces *C. cristatus*.

Ceratolithus lineage evolutionary pattern observed in the sedimentary record of ODP Sites 999 and 1237 indicates that the appearance of *C. finifer* fits a gradualistic model, while the appearance of *C. acutus*, *C. armatus, C. larrymayeri,* and *C. cristatus* fits a punctuated model with lineage splitting.

Finally, environmental oceanic changes that occurred during the Messinian-Pliocene boundary may have produced instability moments that would have caused the compartmentalisation and appearance of new ecological niches potentially leading to the positive selection of new specimens.

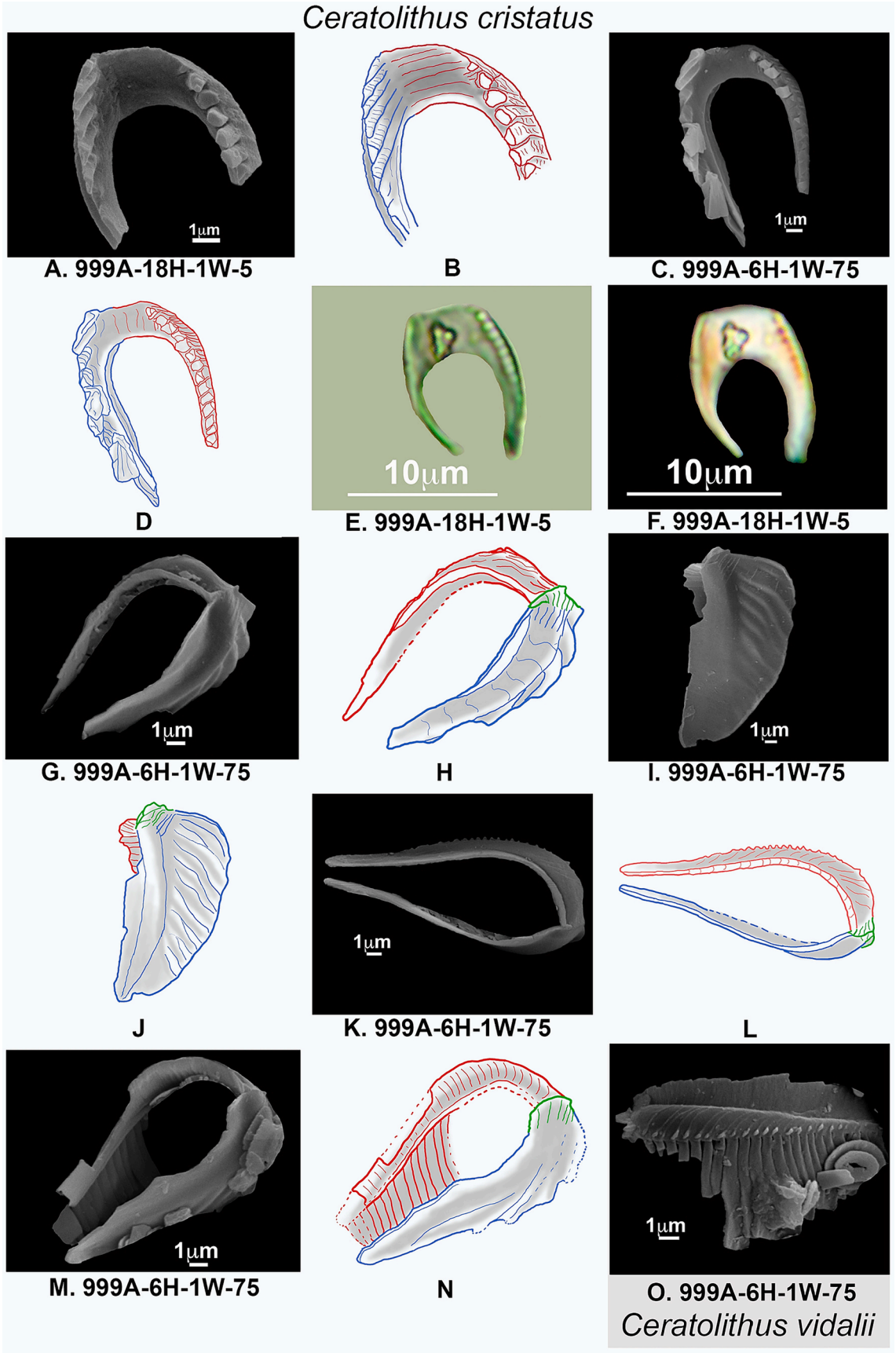

Fig. 14. *Ceratolithus cristatus* and *C. vidalii* morphological variability during Early Pliocene. A, C, G, I, K and M: *C. cristatus* SEM; B, D, H, J, L and N: Drawings after the picture; C to F: described as *C. separatus*; K to N: described as *C. telesmus* E: *C. cristatus* ppl; F: *C. cristatus* xpl the same as E; O*: C. vidalii* SEM.

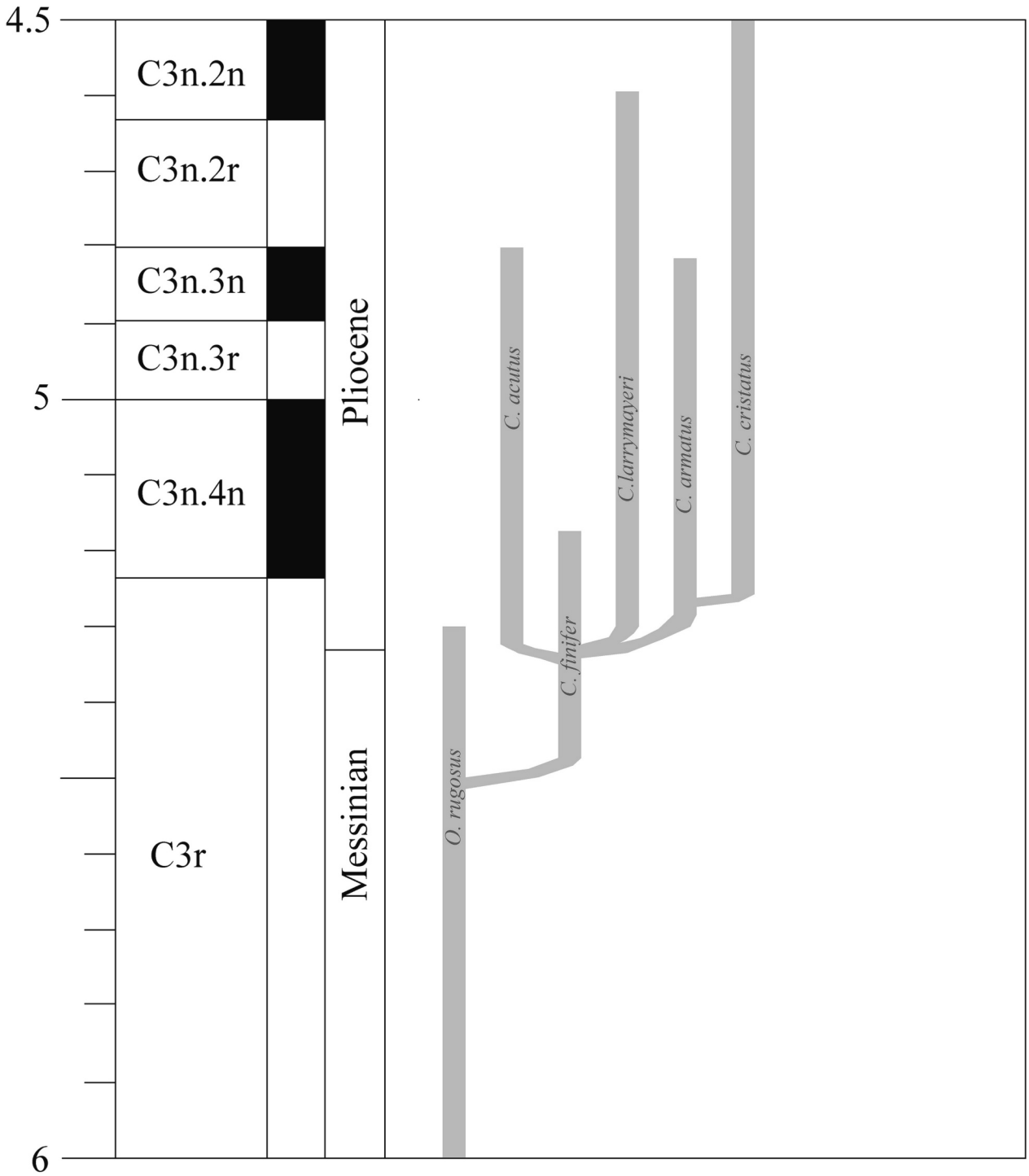

Fig. 15. Biostratigraphic chart showing the Ceratolithus lineage evolution, inferred by the studied samples of ODP holes 999A and 1237 composite. Note the samples calibrated ages seems younger than expected as the *C. acutus* first appearance datum is after the Messinian/Pliocene boundary.

Declaration of Competing Interest

The authors declare that they have no known competing financial interests or personal relationships that could have appeared to influence the work reported in this paper.

Data availability

Data will be made available on request.

Acknowledgments

This work was supported by the projects RTI2018-099489-B-I00 and PID2020-114381GB-I00 (Spanish Ministry of Science, Innovation, and Universities). The authors thank the comments of the early drafts by A. Estévez. We appreciate the assistance of Verónica López and Andrés Amorós of the Microscopy unit and Yolanda López good hand making the SEM samples at the Alicante University. This study was funded by the European Union NextGenerationEU (PRTR-C17.I1) project GVA-THINKINAZUL/2021/039. We also thank the constructive comments

of Isabella Raffi and Jeremy Young. This study used samples provided by the Ocean Drilling Program (ODP).

Appendix A. Supplementary data

Supplementary data to this article can be found online at https://doi.org/10.1016/j.marmicro.2023.102310.

Appendix

Ceratolithus finifer (Theodoridis, 1984) Lancis, Tent-Manclús & Flores n. comb.

Fig. 7G-O; Fig. 8A-O.

Basionym

Triquetrorhabdulus finifer Theodoridis, 1984 *in Utr. Micropaleontol. Bull.* **32**, 271 p.: 89, PI. 11, figs. 7-10. *T. finifer* was recorded as rare in the *C. leptoporus* Subzone B of the D.S.D.P. Site 219.

Remarks

Theodoridis (1984) describes and illustrates this species of *Triquetrorhabdulus* with a very large and crescent-shaped apical blade. The species lacks birefringence. However, it's all about shapes in the most stable position (layout) to see birefringence. Fig. 5 illustrates the proposed gradual morphological change from *Ortorhabdulus* to progressively more stylised specimens that acquire the typical *Ceratolithus* shape with development of initial arms from *Orthorhabdus* blades. The stable position of the nannolith changed during its evolution (Fig. 4), resulting in the older forms with low birefringence and younger ones with moderate to high birefringence.

For this reason, we consider that its assignment to *Triquetrorhabdulus* [now *Ortorhabdulus* Young and Bown, 2014] is not supported, therefore we have reassigned it here to *Ceratolithus*.

The defining characteristics of *C. finifer* n. comb. are elongation, thickening, and to-sinistral bend-end of median wing forming the left proto-arm, and sinistral wing, maintaining laths in the same plane but with its lath-end bent to posterior direction, developing the right proto-arm (Figs. 7G–O and 8A–O).

References

Alcober, J., Jordan, R.W., 1997. An interesting association between *Neosphaera coccolithomorpha* and *Ceratolithus cristatus* (Haptophyta). Eur. J. Phycol. 32, 91–93. https://doi.org/10.1080/09541449710001719385.

Archontikis, O.A., Young, J.R., 2020. Extant *Ceratolithus cristatus* life-cycle observations and taxonomic simplification. J. Nannoplankton Res. 38, 27–39.

Aubry, M.-P., 1988. Handbook of Cenozoic Calcareous Nannoplankton. Book 2: Ortholithae (Catinasters, Ceratoliths, Rhabdoliths). Micropaleontology Press (279 pp.).

Bergen, J.A., 1984. Calcareous nannoplankton from Deep Sea Drilling Project Leg 78A: evidence for imbricate underthrusting at the Lesser Antillian active margin. In: Biju-Duval, B., Moore, J.C., et al. (Eds.), Initial Reports of the Deep Sea Drilling Project, 78A. U.S. Government Printing Office, Washington, pp. 411–445. https://doi.org/10.2973/dsdp.proc.78a.120.1984.

Bickert, T., Haug, G.H., Tiedemann, R., 2004. Late Neogene benthic stable isotope record of Ocean Drilling Program Site 999: implications for Caribbean paleoceanography, organic carbon burial, and the Messinian Salinity Crisis. Paleoceanography 19, PA1023. https://doi.org/10.1029/2002PA000799.

Blair, S., Bergen, J., de Kaenel, E., Browning, E., Boesiger, T., 2017. Upper Miocene -Lower Pliocene taxonomy and stratigraphy of the circum North Atlantic Basin: radiation and extinction of Amauroliths, Ceratoliths and the *D. quinqueramus* lineage. J. Nannoplankton Res. 37, 113–144.

Buitrago-Reina, Y.M., Flores, J., Sierro, F.J., 2010. Calcareous nannofossils Upper Miocene biostratigraphy and biochronology at western equatorial Atlantic (ODP Site 999). Rev. Esp. Micropaleontol. 42, 301–319.

Bukry, D., 1979. Neogene coccolith stratigraphy, Mid-Atlantic Ridge, Deep Sea Drilling Project Leg 45. In: Melson, W.G., Rabinowitz, P.D., et al. (Eds.), Initial Reports of the Deep Sea Drilling Project, 45. U.S. Government Printing Office, Washington, pp. 307–317. https://doi.org/10.2973/dsdp.proc.45.109.1979.

Bukry, D., Bramlette, M.N., 1968. Stratigraphic significance of two genera of Tertiary calcareous nannofossils. Tulane Stud. Geol. Paleontol. 6.

Cros, L., Kleijne, A., Zeltner, A., Billard, C., Young, J.R., 2000. New examples of holococcolith–heterococcolith combination coccospheres and their implications for coccolithophorid biology. Mar. Micropaleontol. 39, 1–34. https://doi.org/10.1016/S0377-8398(00)00010-4.

De Kaenel, E., Berger, J., Browning, E., Blair, S., Boesiger, T., 2017. Uppermost Oligocene to Middle Miocene *Discoaster* and *Catinaster* taxonomy and stratigraphy in the circum North Atlantic Basin: Gulf of Mexico and ODP Leg 154. J. Nannoplankton Res. 37, 215–244.

Dowsett, H.J., Robinson, M.M., 2009. Mid-Pliocene equatorial Pacific sea surface temperature reconstruction: a multi-proxy perspective. Philos. Trans. Soc. A 367, 109–125.

Dowsett, H.J., Robinson, M.M., Foley, K.M., 2009. Pliocene three-dimensional global ocean temperature reconstruction. Clim. Past 5, 769–783.

Filippelli, G.M., Flores, J.A., 2009. From the warm Pliocene to the cold Pleistocene: a tale of two oceans. Geology 37, 959–960. https://doi.org/10.1130/focus102009.1.

Flores, J.A., Sierro, F.J., 1997. Revised technique for calculation of calcareous nannofossil accumulation rates. Micropaleontology 43, 321–324.

Gartner, S., 1967. Calcareous nannofossils from Neogene of Trinidad, Jamaica, and Gulf of Mexico. Univ. Kansas Paleontol. Contr. Pap. 29, 1–7.

Gartner, S., Bukry, D., 1975. Morphology and phylogeny of the coccolithophycean family Ceratolithaceae. J. Res. US Geol. Surv. 3, 451–465.

Gradstein, F.M., Ogg, J.G., Schmitz, M.D., Ogg, G.M., 2012. The Geologic Time Scale 2012. Cambridge University Press. https://doi.org/10.1016/B978-0-444-59425-9.01001-5.

Haug, G.H., Tiedemann, R., 1998. Effect of the formation of the Isthmus of Panama on Atlantic Ocean thermohaline circulation. Nature 393, 673–676. https://doi.org/10.1038/31447.

Haug, G.H., Tiedemann, R., Zahn, R., Ravelo, A.C., 2001. Role of Panama uplift on oceanic freshwater balance. Geology 29, 207. https://doi.org/10.1130/0091-7613(2001)029<0207:ROPUOO>2.0.CO;2.

Haywood, A.M., Valdes, P.J., Sellwood, B.W., 2000. Global scale palaeoclimate reconstruction of the middle Pliocene climate using the UKMO GCM: initial results. Glob. Planet. Chang. 25, 239–256.

Haywood, A.M., Chandler, M.A., Valdes, P.J., Salzmann, U., Lunt, D.J., Dowsett, H.J., 2009. Comparison of mid-Pliocene climate predictions produced by the HadAM3 and GCMAM3 General Circulation Models. Glob. Planet. Chang. 66, 208–224.

Jordan, R.W., Chamberlain, A.H.L., 1997. Biodiversity among haptophyte algae. Biodivers. Conserv. 6, 131–152.

Kameo, K., Bralower, T.J., 2000. Neogene Calcareous Nannofossil Biostratigraphy of Sites 998, 999, and 1000, Caribbean Sea. In: Leckie, R.M., Sigurdsson, H., Acton, G. D., Draper, G. (Eds.), Proceedings of the Ocean Drilling Program. College Station, TX (Ocean Drilling Program), pp. 3–17.

Kamptner, E., 1950. Über den submikroskopischen Aufbau der Coccolithen. Anz. Österr. Akad. Wiss. Math.-Naturw. Kl. 87, 152–158.

Kamptner, E., 1954. Untersuchungen ueber den Feinbau der Coccolithen. Arch. Protistenkd. 100, 1–90.

Kürschner, W.M., van der Burgh, J., Visscher, H., Dilcher, D.L., 1996. Oak leaves as biosensors of late Neogene and early Pleistocene paleoatmospheric CO2 concentrations. Mar. Micropaleontol. 27, 299–312.

Lancis Sáez, C., 1998. El nanoplancton calcáreo de las cuencas neógenas orientales de la Cordillera Bética. University of Alicante.

Lancis, C., Flores, J.-A., 2006. A new biostratigraphically significant calcareous nannofossil species in the Early Pliocene of the Mediterranean. Micropaleontol. https://doi.org/10.2113/gsmicropal.52.5.477.

Lancis, C., Tent-Manclús, J.E., Flores, J.A., 2022. Origin and evolutionary trends of Neogene genera *Amaurolithus* and *Nicklithus* (calcareous nannofossils). Mar. Micropaleontol. 175, 1–15. https://doi.org/10.1016/j.marmicro.2022.102156.

Lancis, C., Tent-Manclús, J.E., Flores, J.A., 2023. A new technique of centrifugation/filtration to improve the quality of the calcareous nannofossil samples for the Scan Electron Microscope. J. Nannoplankton Res. 41 (1), 33–39.

Malmgren, B.A., Berggren, W.A., Lohmann, G.P., 1983. Evidence for Punctuated Gradualism in the Late Neogene *Globorotalia tumida* Lineage of Planktonic Foraminifera. Paleobiology 9 (4), 377–389. http://www.jstor.org/stable/2400580.

Mix, A.C., Tiedemann, R., Blum, Mix, A.C., Tiedemann, R., et al., 2003. Leg 202 summary. In: Blum, P., et al. (Eds.), Proc. ODP, 202 Init. Reports. Ocean Drilling Program, College Station, TX, pp. 1–145.

Naish, T., Powell, R., Levy, R., Wilson, G., Scherer, R., Talarico, F., Krissek, L., Niessen, F., Pompilio, M., Wilson, T., 2009. Obliquity-paced Pliocene West Antarctic ice sheet oscillations. Nature 458, 322.

Norris, R.E., 1965. Living cells of *Ceratolithus cristatus* (Coccolithophorineae). Arch. Protistenkd. 108, 19–21.

Perch-Nielsen, K., 1985. Cenozoic calcareous nannofossils. In: Bolli, H.M., Saunders, J.B., Perch-Nielsen, K. (Eds.), Plankton Stratigraphy. Cambridge Univ. Press, Cambridge, pp. 27–553.

Raffi, I., Backman, J., Rio, D., 1998. Evolutionary trends of tropical calcareous nannofossils in the late Neogene. Mar. Micropaleontol. 35 (1), 17–41. https://doi.org/10.1016/S0377-8398(98)00014-0.

Raffi, I., Backman, J., Fornaciari, E., Pälike, H., Rio, D., Lourens, L., Hilgen, F., 2006. A review of calcareous nannofossil astrobiochronology encompassing the past 25 million years. Quat. Sci. Rev. 25, 3113–3137. https://doi.org/10.1016/j.quascirev.2006.07.007.

Raffi, I., Wade, B.S., Pälike, H., Beu, A.G., Cooper, R., Crundwell, M.P., Krijgsman, W., Moore, T., Raine, I., Sardella, R., Vernyhorova, Y.V., 2020. Chapter 29 - The neogene period. In: Gradstein, F.M., Ogg, J.G., Schmitz, M.D., Ogg, G.M.B.T. (Eds.), Global Time Scales 2020. Elsevier, pp. 1141–1215. https://doi.org/10.1016/B978-0-12-824360-2.00029-2.

Raup, D.M., Crick, R.E., 1981. Evolution of single characters in the Jurassic ammonite Kosmoceras. Paleobiology 7, 200–215.

Ravelo, A.C., Andreasen, D.H., Lyle, M., Lyle, A.O., Wara, M.W., 2004. Regional climate shifts caused by gradual global cooling in the Pliocene epoch. Nature 429, 263.

Raymo, M.E., Grant, B., Horowitz, M., Rau, G.H., 1996. Mid-Pliocene warmth: stronger greenhouse and stronger conveyor. Mar. Micropaleontol. 27, 313–326.
Schmidt, D.N., Thierstein, H.R., Bollmann, J., 2004. The evolutionary history of size variation of planktic foraminiferal assemblages in the Cenozoic. Palaeogeogr. Palaeoclimatol. Palaeoecol. 212, 159–180. https://doi.org/10.1016/j.palaeo.2004.06.002.
Shackleton, N.J., Crowhurst, S., 1997. Sediment fluxes based on an orbitally tuned time scale 5 Ma to 14 Ma, site 926. In: Shackleton, N.J., Curry, W.B., Richter, C., Bralower, T.J. (Eds.), Proc. Ocean Drill. Program, Sci. Results 154. Ocean Drill. Program, Coll. Station. TX, pp. 69–82. https://doi.org/10.2973/odp.proc.sr.154.102.1997.
Shackleton, N.J., Crowhurst, S., Hagelberg, T., Pisias, N.G., Schneider, D.A., 1995. A new Late Neogene timescale: Application to leg 138 sites. In: Pisias, N.G., Mayer, L.A., Janecek, T.R., Palmer-Julson, A., van Andel, T.H. (Eds.), Proc. Ocean Drill. Program, Sci. Results 138. Ocean Drill. Program, Coll. Station. TX, pp. 73–101. https://doi.org/10.2973/odp.proc.sr.138.106.1995.
Sigurdsson, H., Leckie, R.M., Acton, G.D., et al., 1997. 4. Site 999. In: Sigurdsson, H., Leckie, R.M., Acton, G.D., et al. (Eds.), Proc. ODP, Init. Reports. 165. Ocean Drill. Program, Coll. Station. TX, pp. 131–230. https://doi.org/10.2973/odp.proc.ir.165.104.1997.
Sprengel, C., Young, J.R., 2000. First direct documentation of associations of *Ceratolithus cristatus* ceratoliths, hoop-coccoliths and *Neosphaera coccolithomorpha* planoliths. Mar. Micropaleontol. 39, 39–41. https://doi.org/10.1016/S0377-8398(00)00012-8.
Theodoridis, S.A., 1984. Calcareous nannofosils biozonation of the Miocene and revision of the helicoliths and discoasters. Utrecht Micropaleontol. Bull. 32, 271.
Tiedemann, R., Sturm, A., Steph, S., Lund, S.P., Stoner, J.S., 2007. Astronomically calibrated timescale from 6 to 2.5 Ma and benthic isotope stratigraphies, sites 1236, 1237, 1239, and 1241. In: Tiedemann, R., Mix, A.C., Richter, C., Ruddiman, W.F. (Eds.), Proc. Ocean Drill. Program, Sci. Results 202. Ocean Drill. Program, Coll. Station. TX, pp. 1–69. https://doi.org/10.2973/odp.proc.sr.202.210.2007.
Wara, M.W., Ravelo, A.C., Delaney, M.L., 2005. Permanent El Niño-like conditions during the Pliocene warm period. Science 309, 758–761.
Young, J.R., 1998. Neogene. In: Bown, P. (Ed.), Calcareous Nannofossil Biostratigraphy. British Micropalaeontological Society Publications Series. Chapman & Hall, London, pp. 225–265.
Young, J., 2023. Some proposed changes to the systematics of Cenozoic and Mesozoic nannoplankton. J. Nannoplankton Res. 41 (1), 15–25.
Young, J.R., Bown, P.R., 2014. Some emendments to calcareous nannoplankton taxonomy. J. Nannoplankton Res. 33 (1), 39–46.
Young, J.R., Bown, P.R., Lees, J.A. (Eds.), 2023a. *'Ceratolithus'* Nannotax3 Website. International Nannoplankton Association. Accessed 10-July-2023. https://www.mikrotax.org/Nannotax3/index.php?taxon=Ceratolithus&module=ntax_cenozoic.
Young, J.R., Bown, P.R., Lees, J.A. (Eds.), 2023b. *'Ceratolithus armatus*' Nannotax3 Website. International Nannoplankton Association. Accessed 10-July-2023. http://www.mikrotax.org/Nannotax3/index.php?taxon=Ceratolithus%20armatus&module=Coccolithophores.
Young, J.R., Bown, P.R., Lees, J.A. (Eds.), 2023c. *'Ceratolithus atlanticus* ' Nannotax3 Website. International Nannoplankton Association. Accessed 10-July-2023. https://www.mikrotax.org/Nannotax3/cenozoic/Ceratolithus_atlanticus.
Young, J.R., Bown, P.R., Lees, J.A. (Eds.), 2023d. *'Ceratolithus cristatus'* Nannotax3 Website. International Nannoplankton Association. Accessed 10-July-2023. http://www.mikrotax.org/Nannotax3/index.php?taxon=Ceratolithus%20cristatus&module=Coccolithophores.
Young, J.R., Bergen, J.A., Bown, P.R., Burnett, J.A., Fiorentino, A., Jordan, R.W., Kleijne, A., Van Niel, B.E., Ton Romein, A.J., Von Salis, K., 1997. Guidelines for coccolith and calcareous nannofossil terminology. Palaeontology 40 (4), 875–912.
Young, J.R., Davis, S.A., Bown, P.R., Mann, S., 1999. Coccolith ultrastructure and biomineralisation. J. Struct. Biol. 126, 125–215. https://doi.org/10.1006/jsbi.1999.4132.
Young, J.R., Geisen, M., Probert, I., 2005. A review of selected aspects of coccolithophore biology with implications for paleobiodiversity estimation. Micropaleontology 51, 267–288. https://doi.org/10.2113/gsmicropal.51.4.267.